Materials Advances

ROYAL SOCIETY OF CHEMISTRY

PAPER

View Article Online
View Journal | View Issue

Cite this: *Mater. Adv.*, 2025, **6**, 7312

On-demand photoresponsive liposomes-in-gel to prevent UV light-induced cellular damage

Patrick Pan, [b] Shaun W. P. Rees, [b] Darren Svirskis, [a] David Barker, [bc] Geoffrey I. N. Waterhouse [bc] and Zimei Wu *[a]

To achieve prolonged and on-demand sunscreen effects, liposomes containing a lipid with a photoresponsive azobenzene moiety (BisAzo-PC) were constructed and photoprotective effects were demonstrated on a fibroblast cell line. The synthesis of BisAzo-PC was confirmed by FTIR, LC–MS, and ^{1}H NMR. Photoresponsive and thermal properties of BisAzo-PC were studied, revealing a rapid UV-induced *trans–cis* isomerization and a slow *cis–trans* isomerisation. BisAzo-PC liposomes (~120 nm, optimal size for dermal delivery) were prepared and loaded with both hydrophilic (benzophenone-4) and lipophilic (octocrylene) UV filters, achieving high entrapment efficiencies (24.8% and 99.9%) and loading capacities (12.2% and 9.9%, w/w), respectively. The liposomes demonstrated rapid UV filter release triggered by UV irradiation (365 nm), with an extended-release period of 6 hours. Liposomes incorporated into a hydroxypropyl methylcellulose (HPMC)–polyvinylpyrrolidone (PVP)-based bioadhesive hydrogel provided a universal sun protection factor (uSPF) value of 38.1 ± 1.1, exceeding that of a commercial sunscreen of 32.3 ± 0.1. The liposome-in-gel reproducibly protected fibroblasts from UV exposure and reduced intracellular reactive oxygen species (ROS) by 72% for up to 6 hours, accompanied by a 45% reduction of the lipid peroxidation marker malondialdehyde (MDA) and antioxidant enzyme activities of superoxide dismutase (SOD) and glutathione peroxidase (GPx). The results highlight the potential of photoresponsive liposomes-in-gel with extended photoprotective properties to be further translated into a long-acting sunscreen by addressing the main concerns of conventional sunscreens, reducing the need for frequent applications and the risk of systemic absorption of UV filters.

Received 8th May 2025,
Accepted 26th August 2025

DOI: 10.1039/d5ma00460h

rsc.li/materials-advances

1. Introduction

Excessive exposure to ultraviolet (UV) radiation is the cause of 80–90% of all skin cancers, paired with the general difficulties in the treatment of invasive skin cancers, prevention of UV-induced cellular damage remains the best approach for minimizing this significant health burden.[1] The use of sunscreens is recommended as a skin cancer prevention tool and remains a key component of public health campaigns.[2] Traditional sunscreens are successful in preventing both melanoma and non-melanoma cancers,[3] however the rates of aggressive cutaneous melanomas continue to rise,[4] necessitating the development of more effective sunscreens. Furthermore, ongoing concerns regarding the potential harm from systemic absorption of organic UV filters need to be addressed.[5,6] Controlled drug delivery systems offer an attractive platform for extending and improving the efficacy of traditional sunscreens and UV filters by addressing the main drawback of the current sunscreen products (*i.e.* the requirement for frequent reapplication),[7] while minimising their potential for systemic absorption and subsequent risk of systemic side effects.[8]

Phototriggered drug release systems have attracted considerable interest in recent years as a controlled drug delivery platform due to the non-invasiveness of light as a stimulus. Such photoresponsive delivery systems are designed to undergo change upon receiving photons with suitable energy, offering many advantages over other stimuli-responsive formulations for drug delivery since photochemical processes do not require additional reagents or catalysts, with the majority of by-products, if any, being harmless.[9] Well-designed delivery systems can realise a high degree of temporal and spatial control for the release of encapsulated therapeutics in an on-demand manner.[9] Of the photosensitive moieties commonly used to impart photoresponsiveness to drug delivery systems,

[a] *School of Pharmacy, Faculty of Medical and Health Sciences, The University of Auckland, Auckland, New Zealand. E-mail: t.pan@auckland.ac.nz, z.wu@auckland.ac.nz, d.svirskis@auckland.ac.nz; Tel: +64-9-9231709*
[b] *School of Chemical Sciences, Faculty of Science, The University of Auckland, Auckland, New Zealand. E-mail: sree168@aucklanduni.ac.nz, d.barker@auckland.ac.nz, g.waterhouse@auckland.ac.nz*
[c] *The MacDiarmid Institute for Advanced Materials and Nanotechnology, Wellington, New Zealand*

azobenzene and its derivatives stand out due to their reversible *trans*-to-*cis* isomerization process, potentially offering a platform for triggered drug release in a multi-pulsatile manner.[9,10] One such photochromic lipid, 1,2-bis(4-(*n*-butyl)phenylazo-4′-phenylbutyroyl)phosphatidylcholine (BisAzo-PC), has seen use in the development of photoresponsive liposomes, but clinically relevant pulsatile release has yet to be achieved.[11–16]

Liposomes are phospholipid nanovesicles with a bilayer membrane structure and have been extensively studied as vehicles for drug delivery. Recent research has demonstrated the potential of the light-controlled rupture of liposomes, wherein photosensitive moieties incorporated into the lipid bilayer can initiate release of their cargo upon light irradiation for localized drug release.[17] Liposomes can simultaneously carry both hydrophilic and lipophilic compounds,[18,19] and when topically applied, act as a local drug reservoir on the skin, thereby diminishing the risk of systemic side effects of drug delivery.[20] However, effective delivery methods needs to be discovered which allow light-triggered liposomes to remain on the skin for extended periods.

Hydrogels are homogeneous semisolids consisting of a water-swollen hydrophilic polymer three-dimensional network. Due to their high water content, hydrogels can effectively support the sustained delivery action of liposomes. Binary hydrogels in particular, are often designed to have a high degree of bioadhesiveness which can prolong drug release.[21,22] The combination of both liposomes and hydrogels provides a synergistic effect by extending the liposomes' retention time on the skin while further prolonging drug release to achieve a highly localized dermal delivery platform for minimizing systemic drug absorption and side effects.[23,24]

This research aimed to develop a photoresponsive liposome for the simultaneous UV light-triggered delivery of two UV filters (benzophenone-4 and octocrylene). To enhance the retention on skin, liposomes were incorporated into a bioadhesive hydrogel,[22] resulting in a formulation with improved photoprotective effects compared to a conventional sunscreen along with prolonged and on-demand phototriggered release properties. Primary neonatal human dermal fibroblasts were used to test the biological response to UV irradiation by measuring various oxidative stress markers, and compared the liposome-in-gel formulations. Such prolonged and phototriggered release properties were expected to offer improved UV protection for sunscreen users.

2. Materials and methods

Dipalmitoyl phosphatidylcholine (DPPC) and hydrogenated soybean phosphatidylcholine (HSPC) (PHOSPHOLIPON® 90 H) were kindly gifted by Lipoid GmbH (Ludwigshafe, Germany). Octocrylene, benzophenone-4, cholesterol, hydroxypropyl methylcellulose K100 (HPMC), polyvinylpyrrolidone K25 (PVP), 2′,7′-dichlorofluorescein diacetate (DCF-DA), malondialdehyde (Cat. No. MAK085), superoxide dismutase (Cat. No. 19160), and glutathione peroxidase (Cat. No. MAK437) assay kits, and cellulose dialysis bags (MWCO = 14 000 Da) were purchased from Sigma-Aldrich (Auckland, New Zealand). Cell Counting Kit 8 (CCK8) assay was purchased from Abcam (United Kingdom).

Sodium phosphate dibasic and sodium phosphate monobasic were used to prepare a 0.1 M phosphate buffered saline (PBS) solution, with the final pH adjusted to 5.5 using hydrochloric acid. Milli-Q water was obtained from a Millipak® 0.22 Em system (Millipore Corporation, Bedford, MA, USA). All other solvents and reagents used were of analytical grade. The UV lamp used for irradiation in all experiments was a Spectroline Model SB-100P/FA High-Intensity UV Lamp (365 nm) with specifications for UVA radiation intensity of 4800 μW cm^{-2} (at a distance of 38 cm).

2.1 Synthesis and characterisation of photoresponsive lipid BisAzo-PC

2.1.1 Synthesis of BisAzo-PC. Photoresponsive lipid 1,2-bis(4-(*n*-butyl)phenylazo-4′-phenylbutyroyl)phosphatidylcholine (BisAzo-PC) was synthesized by adapting literature methods and full details are described in the SI (SI1),[25–28] with modifications, using Oxone®, 4-butylaniline, 4-(4-aminophenyl)butyric acid, and *sn-glycero*-3-phosphocholine (Sigma-Aldrich, Auckland, New Zealand), and *N*,*N*′-Carbonyldiimidazole and 1,8-diazabicyclo[5.4.0]undec-7-ene (DBU) (AK Scientific, CA, USA).

The three-step reaction scheme is outlined as follows (Fig. 1). First, oxidation of **4-butylaniline** using Oxone® was conducted to obtain **1-butyl-4-nitrosobenzene.** Condensation of **1-butyl-4-nitrosobenzene** with **4-(4-aminophenyl)butyric acid** using glacial acetic acid then gave the azobenzene-containing acid, (***E***)**-4-(4-((4-butylphenyl)diazenyl)phenyl)butanoic acid**. The acid was then converted into the target compound **1,2-bis(4-(*n*-butyl)phenylazo-4′-phenylbutyroyl)phosphatidylcholine** (BisAzo-PC) using a mixed anhydride acylation of *sn-glycero*-3-phosphocholine, using DBU as a catalyst. Flash chromatography was used for purification of BisAzo-PC using silica gel (pore size 60 Å, 40–63 μm particle size, 230–430 mesh particle size). Synthesized BisAzo-PC were stored in glass vials protected from light at −20 °C for storage and used within 3 months.

2.1.2 Structure confirmation and thermal properties of BisAzo-PC. To elucidate and confirm the synthesized molecular was BisAzo-PC, nuclear magnetic resonance (NMR), high-resolution mass-spectroscopy (HRMS), and Fourier-Transform Infrared (FTIR) spectroscopy were used. The NMR spectra were recorded on a Bruker Avance 400 MHz spectrometer at ambient temperature. Chemical shifts (δ) are reported relative to the solvent peak of chloroform (δ 7.26 for ^{1}H and δ 77.0 for ^{13}C) or DMSO (δ 2.50 for ^{1}H and δ 39.5 for ^{13}C). The ^{1}H NMR data are reported as chemical shift (δ), relative integral, multiplicity (s, singlet; d, doublet; dd, doublet of doublets; ddd, doublet of doublet of doublets; t, triplet; m, multiplet; and br, broad peak), coupling constant (J, Hz), and the assignment of the atom. ^{13}C NMR data are reported as chemical shift (δ) and assignment of the atom. All NMR assignments were performed with HSQC and HMBC experiments from integrated software. HRMS was carried out by electrospray ionization (ESI) on a MicroTOF-Q II mass

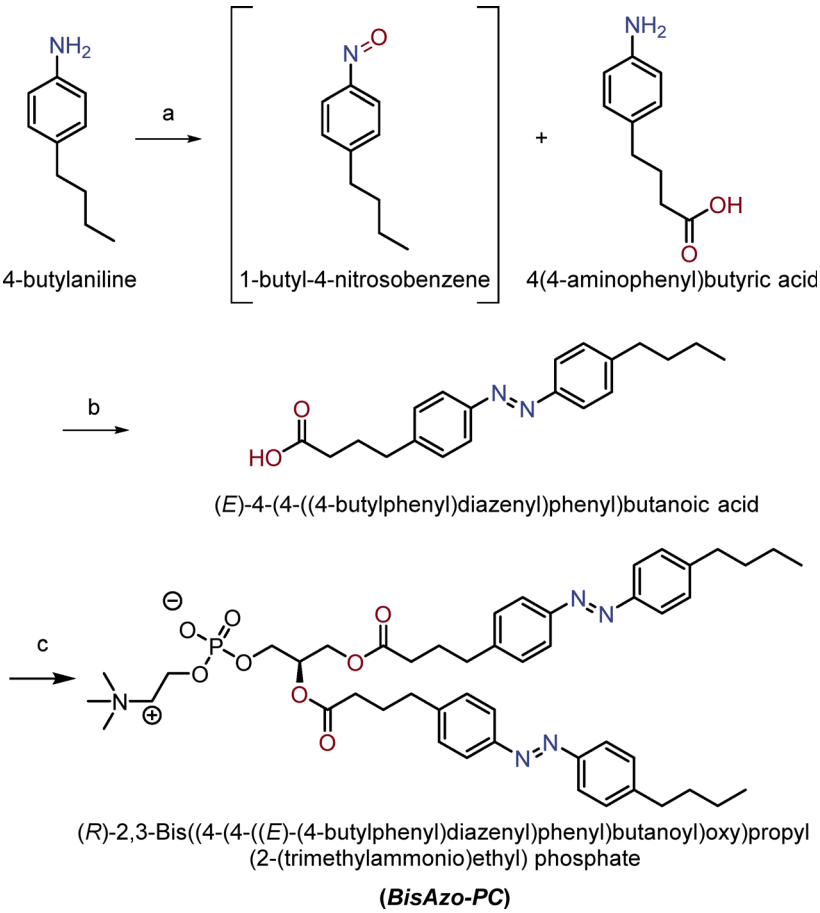

Fig. 1 Reaction schematic for the synthesis of BisAzo-PC through an azo-condensation of 1-butyl-4-nitrosobenzene with 4-(4-aminophenyl)butyric acid, followed by a mixed anhydride acylation of *sn-glycero*-3-phosphocholine. Reagents and conditions: (a) oxone in H_2O, CH_2Cl_2, rt, 24 h, aq. 1 M HCl; (b) glacial acetic acid, 4-(4-aminophenyl)butyric acid in glacial acetic acid, rt, 24 h, 50% (two steps); (c) CDI, CH_2Cl_2, 3 h, rt, *sn-glycero*-3-phosphocholine, 1,8-diazabicyclo[5.4.0]undec-7-ene, DMSO, rt, 2 d, 74%.

spectrometer. Freshly synthesized and dried samples were analysed with a Bruker Alpha Eco-ATR FTIR Spectrometer with OPUS 8.7.41 ALPHA software (Bruker, Mannheim, Germany).

The glass transition temperature (T_c) and melting point (T_m) of BisAzo-PC, the key parameters of phospholipids determining the payload release from liposomes, were measured using a differential scanning calorimeter (DSC) Q2000 + RCS40 (TA Instruments, Delaware, USA), with a nitrogen flow rate of 20 mL min^{-1} and an initial temperature of 20 °C increasing at a rate of 10 °C min^{-1} to 150 °C.

2.1.3 Photoresponsive properties of BisAzo-PC. To investigate the photoresponsive properties of BisAzo-PC, the UV-Vis absorption spectra (280–400 nm) of pure BisAzo-PC was measured before and after UV irradiation using a T90+ UV-Vis spectrophotometer (PG Instruments, Lutterworth, UK) at 25 °C. Briefly, BisAzo-PC in methanol (0.15 mmol L^{-1}) was prepared in a 10 mm quartz cuvette, and the absorption spectrum taken before irradiation at a wavelength of 365 nm (0 min), and at the subsequent time points: 1, 2, 3, 4, 5, 6, 7, 8, 9, 10, and 15 min. Irradiation was then ceased and the sample protected from light to allow for isomeric relaxation and spectra taken at 15, 30, 60, 120, and 1080 min. The photochemical fatigue of BisAzo-PC was investigated by measuring the change in maximum absorbance over multiple cycles of UV irradiation (5 min) and relaxation (120 min).

2.2 Preparation of photoresponsive liposomes loaded with UV filters

Photoresponsive liposomes were prepared using the thin-film hydration method. Briefly, either DPPC or HSPC, cholesterol, and BisAzo-PC (84 : 10 : 6, mol%) were dissolved in 1 mL chloroform/methanol (9 : 1, v/v) with lipophilic octocrylene (10 mg mL^{-1}) in a round-bottom flask. The solvent was then evaporated at 60 °C in a rotary evaporator (Rotavapor, Büchi, Germany) to form a thin-film and flushed with nitrogen gas to remove residual solvent. The film was hydrated using 3 mL of pre-warmed benzophenone-4 solution (10 mg mL^{-1} in PBS) to passively load the hydrophilic UV filter and mixed for 1 h (final lipid concentration = 30 mg mL^{-1}). Resulting multilamellar vesicles were sized down by heating the liposome suspension to 60 °C and sonicated for 120 s (40% intensity, 0.4 duty) with a SONOPULS HD2070 probe sonicator (Bandelin electronic GmbH & Co. KG, Berlin, Germany), and annealed at room temperature for 1 h.

Unentrapped octocrylene and benzophenone-4 were separated from the liposomes using ultracentrifugation (Sorvall, Beckman Coulter, Pasadena, CA) at 41 000 × *g* for 15 min at 4 °C. The supernatant was removed and the dry pellets stored at 4 °C for subsequent use (within 24 h of preparation). Liposome pellets were resuspended in PBS to achieve a final lipid concentration of 30 mg mL^{-1} immediately before use.

2.3 Characterization of the liposomes

2.3.1 Particle size, zeta potential, and morphology. The size and size distributions of the prepared liposomes were determined by dynamic light scattering using a Zetasizer Nano ZS (Malvern Instruments, Malvern, UK). Samples were diluted 100-fold with Milli-Q water, loaded into a DTS1070 capillary cuvette, and measured at 25 °C with a detection angle of 173° and laser wavelength of 633 nm. Liposome size and distribution was expressed in terms of intensity (*Z*-Ave) and polydispersity index (PDI), respectively. The zeta potential (ZP) of samples were simultaneously measured under the same conditions. Measurements from three independent samples were recorded to obtain the mean values.

Liposome morphology was investigated using a transmission electron microscope (TEM). Both DPPC (DPPC:Chol:BisAzo-PC; 84, 10, 6 mol%) and HSPC-based liposomes (HSPC:Chol:BisAzo-PC; 84, 10, 6 mol%) negatively stained with uranyl acetate 1% (UA) solution by dilution of the sample at 1 : 20, then placed onto a copper grid for 60 s. Excess liposome suspension was drawn off using filter paper (Whatman Inc., Clifton, NJ, USA) and dried overnight under vacuum protected from light. Visualization was performed with a Zeiss EM 900 Transmission Electron Microscope (Carl Zeiss AG, Oberkochen, Germany) operating at 120 kV.

2.3.2 Entrapment efficiency and UV filter loading. The entrapment efficiency (EE) and UV filter loading capacity (LC) of encapsulated benzophenone-4 and octocrylene from freshly prepared liposome pellets were measured directly after inducing vesicle lysis. Immediately after the formulations were prepared, lipid pellets were resuspended in Triton X-100 (0.2%) to lyse the vesicles, the samples filtered (0.45 μm) and then diluted with mobile phase and analysed by HPLC to determine the total amount of encapsulated UV filters in the liposomes.[29] The EE and LC were then calculated using the following formulae.

$$\text{Entrapment efficiency (\%)} = \frac{\text{final mass of encapsulated UV filter}}{\text{initial mass of UV filter}} \times 100$$

$$\text{Loading capacity (\%)} = \frac{\text{final mass of encapsulated UV filter}}{\text{final mass of UV filter encapsulated particles}} \times 100$$

Both UV filters were simultaneously quantified using a previously established HPCL assay.[29] A Shimadzu LC-20 Prominence Series HPLC (Shimadzu, Kyoto, Japan) equipped with a LC-20AD quaternary pump, a DGU-20A5R degassing unit, a SIL-20AC auto-sampler (set at 4 °C), a CTO-20AC column oven (40 °C), and a SPD-M20A diode array detector was used. Chromatographic separation was achieved on an Inertsil® ODS-3V C-18 column (250 mm × 4.60 mm ID, particle size 5 μm, pore size 100 Å) (GL Sciences Inc., Tokyo, Japan). The mobile phase consisted of acetonitrile–methanol-Milli-Q water + TFA (0.2% v/v) (20 : 67 : 13, v/v/v), at a flow rate of 1 mL min^{-1}, with an injection volume of 10 μL. The eluted compounds were monitored at 285 nm (benzophenone-4) and 305 nm (octocrylene).[29]

2.3.3 Transition temperature of liposome membranes. The thermal properties of pure BisAzo-PC, and DPPC- and HSPC-based liposome formulations dried under vacuum were investigated by thermogravimetric analysis (TGA) and differential scanning calorimetry (DSC). No UV filters were encapsulated for these studies.

TGA was carried out using a PerkinElmer TGA 8000 (PerkinElmer Inc., Waltham, MA, USA). Briefly, crucibles were loaded with sample (between 1–3 mg) and then heated from 20 °C to 150 °C at a rate of 10 °C min^{-1}. Nitrogen gas purging at a flow rate of 10 mL min^{-1} was used for all samples in a non-pressurized furnace. Thermograms were analysed with the Pyris Software v13.2.1.0007 (2015).

DSC analysis was performed on dry liposome samples (10 mg) hermetically sealed into T-zero aluminium pans loaded into a Q2000 + RCS40 DSC (TA Instruments, Delaware, USA). The heating rate was 10 °C min^{-1} and the temperature range was from 10 to 150 °C, with a nitrogen flow rate of 20 mL min^{-1}. TA Instruments Universal Analysis 2000 software was used to analyse the differential thermograms. The phase transition temperature (T_c) is identified using the half-height analysis method, and the melting point identified as the lowest point in the thermogram.

2.3.4 Phototriggered UV filter release. After liposome preparation, the DPPC- and HSPC-based photoresponsive formulations were subjected to UV irradiation at 365 nm to trigger cargo release using a Spectroline Model SB-100P/FA High-Intensity UV Lamp (UVA radiation intensity of 4800 μW cm^{-2} at a distance of 38 cm). Non-photoresponsive liposomes prepared without BisAzo-PC were used as the control.

Regenerated cellulose dialysis bags were chosen to hold photosensitive liposomes while drug release studies were undertaken. The transmittance of the dialysis bags was first measured to validate the suitability of the material for phototriggered drug release of photosensitive liposomes held inside the bag. A single layer of dialysis tubing was cut and rehydrated in PBS, before being stretched over a custom plastic bracket fitted into a Varioskan LUX microplate reader with SkanIt Software 6.0.2 (Thermo Fisher Scientific, Waltham, MA, USA). The absorbance spectrum between 200 and 800 nm was obtained at a temperature of 33 °C and converted to transmittance with the software.

Liposome formulations (1 mL) were loaded and sealed into dialysis bags before being submerged in PBS (50 mL) in a doubled jacketed borosilicate glass reaction vessel connected to

a circulatory water bath to maintain a temperature within the vessel of either 23, 33, or 37 °C. The media was stirred with a magnetic bar at 800 rpm. An optical grade quartz plate was placed above the reaction vessel to minimize media loss by evaporation while permitting 100% transmission of UV light. Aliquots were withdrawn at predetermined intervals and replaced with fresh PBS, before analysis by HPLC. The assessment of the photoresponsive property of the liposomes involved measuring the release of benzophenone-4 encapsulated in the aqueous cavity before and after UV irradiation.

2.3.5 Physical stability. The stability of the liposome suspensions was evaluated by storing at 4 °C for 90 days. Measurements were taken *via* dynamic light scattering every 10 days, monitoring for changes in particle size, PDI, and zeta potential over time.

2.4 Preparation of hydrogels and integration with liposomes

A binary adhesive hydrogel (H12P6) was used as the topical base for the liposomes.[22] Briefly, HPMC or PVP were weighed, mixed, and dispersed in half the necessary amount of PBS (pre-warmed to 80 °C), followed by vigorous stirring for 10 min to obtain a well-dispersed mixture. Further PBS (at room temperature) was then slowly added to produce the final desired concentration of 12% HPMC and 6% PVP (w/w).[22] Gels were stored overnight in capped bottles at 4 °C to allow air bubbles to escape. Liposomes were incorporated into pre-formed H12P6 hydrogels by directly adding liposome suspension to the gel followed by gently mixing.[24]

2.5 Skin permeation, retention, and deposition

2.5.1 Skin preparation. Freshly excised porcine skin from the flank was collected within 2 h of slaughter (age 5–6 months) from a local abattoir (Auckland Meat Processors Ltd), wrapped and transported with ice for immediate preparation and same day use in the laboratory. Excessive subcutaneous fat was carefully removed to obtain full-thickness skin. The epidermis was then separated by the heat separation method.[30] Briefly, excised skin sections were immersed in PBS (60 °C) for 60 s, transferred into cold PBS for 60 s, then excess liquid dried. The epidermis was carefully peeled off from the dermis in a single sheet with an average thickness of 1.6 mm ± 0.2 mm (n = 9).

The integrity of excised skin was determined by measurement of the electrical resistance across the isolated epidermis mounted onto standard glass static diffusion with PBS in the receptor and donor chambers. Measurements were taken 30 min after setup to ensure temperature and humidity equilibration to ambient conditions. Probes were submerged into the media above and below the skin and the electrical resistance recorded, correcting for the permeation surface area (1.77 cm^2), and expressed as kΩ cm^{-2}. The cut-off electrical resistance value for indication of good integrity was 1.18 kΩ cm^{-2}, and any skin below this was discarded and replaced.[31] Details of the cell assembly can be found in the OECD Test Guideline No. 428.[32] Validated epidermis sections were used within 12 h for skin permeation, retention, and deposition studies of UV filters.

2.5.2 Permeation. Percutaneous permeation studies through the epidermis as performed on a DHC-6T dry heating transdermal diffusion system (Logan Instruments Corp., Somerset, NJ, USA). The epidermis was positioned between the donor and receptor compartments with the upper stratum corneum oriented towards the donor cell, both compartments filled with PBS, then the skin integrity checked using electrical resistance, as described below. Care was taken during setup to avoid and remove air pockets between the underside of the epidermis and receptor medium. The receptor cells were maintained at 33 ± 0.5 °C and stirred with a magnetic bar at 500 rpm. The effective diffusion area was 1.77 cm^2. All skin samples were left for 3 h to equilibration before filling of the donor cell for the start of the permeation study. Samples were taken in triplicate. Briefly, at time zero, 1 mL of test sample was applied directly into the donor cell and sealed by taping a small quartz slide over the orifice to prevent evaporation. At predetermined time intervals, 200 μL of receptor fluid was sampled and replaced with fresh PBS, then analysed with HPLC.

The permeation of free drug in H12P6 hydrogel containing benzophenone-4 (2.5 mg) and octocrylene (10 mg), and two UV filter loaded liposomes – a non-photoresponsive HSPC-based liposome, and a photoresponsive HSPC-based liposome, also suspended in H12P6 gel (50/50, w/w). Samples were tested while fully exposed to ambient light.

2.5.3 Retention. After permeation studies with the Franz-Cell, the remaining epidermis was then removed from the system, rinsed three times with PBS and excess fluid drawn off with filter paper. The isolated epidermis was then frozen by dipping briefly in liquid nitrogen before homogenizing by pulverization in a Thomas Teflon pestle tissue homogenizer (Arthur H. Thomas Company, Philadelphia, PA, USA). Small amounts of liquid nitrogen were added during the process to assist producing a fine powder-like form from the epidermis. The powdered skin was then extracted in methanol before analysis with HPLC.

2.5.4 Deposition. Full-thickness skin was obtained from excised porcine skin by removing the underlying subcutaneous adipose and connective tissue with scalpels to isolate the stratum corneum, epidermis, and dermis. The skin was then rinsed 3 times with fresh PBS, excess fluid drawn off with filter paper, and the surface dried briefly using warm air and inspected for physical lesions. Only healthy intact skin was used.

The optimized HSPC-based photoresponsive formulation was assessed (HSPC:Chol:BisAzo-PC; 84, 10, 6 mol%) in gel, by suspending liposomes in H12P6 gel (50/50, w/w).

Sample (0.5 g) was applied to the surface of the dried full-thickness skin (cut an area of 1 cm^2) and left for 2 h before being rinsed 3 times with Milli-Q water and any excess fluid drawn off with filter paper and dried briefly using warm air. The stratum corneum was then removed by the tape stripping method. Briefly, 1 cm^2 sections of Scotch™ 810 Magic Tape (3M, Auckland, New Zealand), were placed onto the stratum corneum and a 2 kg weight was placed above for 5 s. Afterwards, the tape was removed with a sharp upward movement to remove corneocytes from the skin surface for twelve consecutive strippings. Each tape was weighed and immersed in

toluene for 5 min, followed by vortexing and sonication for 15 min for extraction and then centrifuged at 8000 × *g* for 5 min. The supernatant was filtered (0.45 μm) before analysis by HPLC.

2.6 Cellular responses to UV light and photoprotective effects of photoresponsive liposome-in-gel

2.6.1 Cell culture, UV irradiation, and formulation treatment. Primary neonatal human dermal fibroblast (HDFn) cells were purchased from Thermo Fisher Scientific (C-004-5C; Victoria, Australia), and cultured in Dulbecco's Modified Eagle's Medium (DMEM) supplemented with fetal bovine serum (10%, v/v), 100 U mL^{-1} of penicillin, and 100 μg mL^{-1} streptomycin. All cells were incubated under standard conditions at 37 °C and 5% CO_2. Culture media was replaced every 2 days. Cells were sub-cultured after reaching 80% confluency while in the log phase of cell growth, and passages were limited to a maximum of 11 for all experiments.

Before UV irradiation, HDFn were seeded in 96-well microplates (2×10^4 cells per well) with 200 μL DMEM and incubated for 24 h for cells to adhere. To apply each treatment and to protect the underlying cells, seeded wells were covered with an optical grade quartz plate. Formulations were spread on the plate at 2 mg cm^{-2} and air-dried for 30 min. Irradiations were performed using a Spectroline Model SB-100P/FA High-Intensity UV Lamp (365 nm; UVA radiation intensity of 4800 μW cm^{-2} at a distance of 38 cm).

The following formulations were tested: (i) a commercial sunscreen (*Cicatricure* Gold Day) with SPFE (Genomma Lab, TX, USA), (ii) H12P6 binary gel; (iii) H12P6 binary gel with UV filters (10% w/w of each benzophenone-4 and octocrylene); (iv) H12P6 binary gel with photoresponsive liposomes loaded with benzophenone-4 and octocrylene; (v) H12P6 binary gel with blank non-photoresponsive liposomes; (vi) H12P6 binary gel with blank photoresponsive liposomes. Unirradiated cells were kept in the dark at room temperature as controls.

2.6.2 Cell viability and morphology analysis. Viability of HDFn before and after UV irradiation was assessed using a CCK8 assay. Cells were exposed to UV irradiation for 2.5, 5, 10, 15, and 30 min before the addition of 10 μL of WST-8 and incubated for 1 h. The absorbance was measured at 460 nm before, immediately after, and 24 h after UV irradiation. Cell viability was determined by calculating the number of viable cells with reference to a simultaneously obtained calibration curve.

2.6.3 Intracellular ROS formation. Total intracellular ROS levels were measured using the fluorogenic compound 2′,7′-dichlorofluorescein diacetate (DCF-DA). Cells in 96-well plates were incubated with 10 μM DCF-DA for 30 min at 37 °C then washed twice with 1× PBS and fresh media added to each well. Treatments were applied to protect the underlying cells as described above prior to UV irradiation (10 min). Fluorescence intensity was measured every hour over 6 h at Ex/Em = 495/530 nm in a Varioskan LUX microplate reader (Thermo Fisher Scientific, Victoria, Australia). The change in fluorescence intensity relative to untreated control cells expressed in Relative Fluorescence Units (RFU).

2.6.4 Oxidative stress markers. HDFn cells were seeded into 24-well plates (20 000 cells per well) and allowed to adhere for 24 h before being subjected to UV irradiation (10 min) and protected by formulations described previously, before the cells were harvested with a cell scraper for analysis of malondialdehyde (MDA) as a marker for lipid peroxidation, and the antioxidant enzymes superoxide dismutase (SOD) and glutathione peroxidase (GPx), as response biomarkers of the cellular defence mechanisms for neutralising ROS. MDA levels and antioxidant SOD and GPx enzyme activities were quantified using the respective assay kits according to the manufacturer's protocols and measured in a microplate reader.

Membrane lipid peroxidation (MDA). MDA generated from the peroxidation of polyunsaturated fatty acids due to free radicals were quantified as a marker for membrane lipid peroxidation of omega-3 and omega-6 fatty acids indicative of plasma membrane damage.[33] Cells were treated then harvested as detailed above before analysis. Briefly, cells were homogenized on ice in 300 μL of MDA Lysis Buffer and 3 μL butylated hydroxytoluene. The lysate was then centrifuged at 13 000 × *g* for 10 min at 4 °C to remove insoluble material. Aliquots of the supernatant (200 μL) from each homogenized sample were placed into microcentrifuge tubes, then 600 μL of thiobarbituric acid solution was added to each sample for incubation at 95 °C for 60 min. Samples were then cooled to room temperature in an ice bath for 10 min then the absorbance measured at 532 nm using a microplate reader. MDA levels were expressed as concentrations (nmol mL^{-1}).[34]

Antioxidant enzyme activities (SOD and GPx). The antioxidant protective capacity against free radicals superoxide radical ($^*O_2$) or singlet oxygen radical ($^1O_2^-$) is determined by SOD enzyme activity, and against peroxide (H_2O_2) by GPx.[35] Cells were treated then harvested as detailed above before analysis. The enzymatic activities of SOD and GPX were then determined by biochemical methods described below.

Superoxide dismutase. Intracellular antioxidant SOD enzyme activities were determined using xanthine oxidase and the water-soluble tetrazolium WST-1.[36] Briefly, harvested cells were lysed in ice cold Tris/HCl (0.1 M, pH 7.4) containing 0.5% Triton-X 100, 5 mM β-ME, and 0.1 mg mL^{-1} PMSF. The cell lysate was then centrifuged at 13 000 × *g* for 10 min at 4 °C to remove debris. Aliquots of the supernatant (20 μL) were then added to the Enzyme Working Solution and/or the WST Solution provided in the assay kit. Microplates were then incubated at 37 °C for 20 min and the absorbance measured at 450 nm using a microplate reader.

Glutathione peroxidase. The GPx activity was determined indirectly by a coupled reaction with glutathione reductase.[37] Briefly, harvested cells were homogenized on ice in 200 μL of cold 1× PBS (pH 7.4) and centrifuged at 13 000 × *g* for 10 min at 4 °C to pelletise the debris. The supernatant (10 μL) was then added to each well in a 96-well microplate. The Working Reagent (90 μL) and Substrate Solutions (100 μL) provided in the assay kit were then quickly added to each sample, the

microplates gently mixed, and the absorbance at 340 nm immediately measured, and measured again after a reaction time of 4 min. GPx Enzyme Activity was then calculated and expressed as the quantity of active enzyme present. A standard curve was also prepared to ensure the GPx activity in the samples was within the linear range of 40–800 U L^{-1}. No dilutions of the samples were required to achieve this range.

2.7 Universal sun protection factor of liposomes-in-gel

To estimate the SPF of each formulation, the universal sun protection factor (uSPF) was calculated. Briefly, formulations (2 mg cm^{-2}) were placed in the centre of a fused quartz slide (50 × 50 × 1 mm; Alpha Nanotech Inc., Canada), after which another slide was placed on top and an even force applied at the centre using callipers until the thickness of the formulation was 0.1 mm between the two quartz slides. The quartz slides were then fitted in a 3D printed custom plastic bracket and then placed into a microplate reader for measurement.

Absorption spectra of each formulation were collected between 280 and 400 nm, which covered both the UVA and UVB ranges. The uSPF values were then calculated using the equation below.[38]

$$\text{uSPF} = \frac{100}{\text{Average sum transmission value}}$$

where the average sum transmission value is the area under the curve of the absorption spectrum divided by 120 (corresponding to the UV wavelength range 280–400 nm).

2.8 Statistical analysis

All experiments were repeated in triplicate, with the data expressed as the mean ± standard deviation (SD). Statistical comparison between groups was carried out using one-way analysis of variance (ANOVA) and Tukey HSD procedure as a post-hoc test with GraphPad Prism (Version 9, GraphPad Software, La Jolla, CA, USA). Differences in p-value < 0.05 were considered statistically significant.

3. Results

3.1 Structural confirmation and characteristics of BisAzo-PC

3.1.1 Structural confirmation of BisAzo-PC. The synthesized BisAzo-PC samples were analysed using the ATR-FTIR method. The spectra were collected over the wavenumber range of 4000 to 400 cm^{-1} at a resolution of 4 cm^{-1} to confirm the expected functional groups of the synthesised compounds (Fig. 2).

The structure of intermediate compounds and BisAzo-PC was also elucidated using ^{1}H and ^{13}C NMR (Fig. S2–S5) with clear evidence of the introduction of two azo-lipids. In the ^{1}H NMR the integration values show a 2 : 1 ratio between the lipid fragments and glycerol component and in the ^{13}C NMR two signals at ~173 ppm indicate ester linkages between the lipids and the glycerol alcohol. HRMS determined the correct molecular formula for BisAzo-PC [$C_{48}H_{64}N_5O_8P$] and has a calculated monoisotopic mass of 870.02 Da, with the determined mass of the product at 870.45 g mol^{-1} (Fig. S6). It is

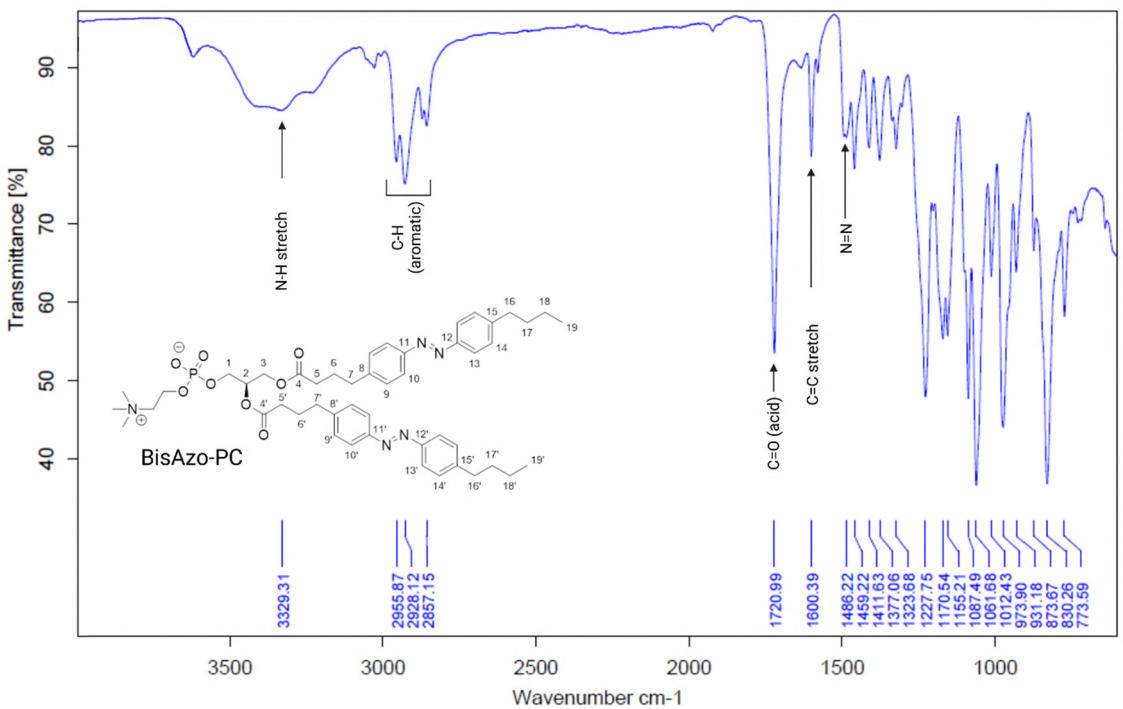

Fig. 2 FTIR spectrum of BisAzo-PC. The 1500 cm^{-1} band is assigned to a N=N stretching vibration, whilst a strong band due to C=C stretching vibration of the aromatic rings was evident in the region around 1600 cm^{-1}. An intense carbonyl (C=O) stretching mode at 1721 cm^{-1} could readily be assigned to ester functional groups in BisAzo-PC. Aromatic C–H stretching modes were seen at 3000–3100 cm^{-1}.

evident from the NMR, mass spectrometry, and FTIR analyses that BisAzo-PC was successfully synthesized with all characterization data in agreement with the required compound.

3.1.2 Thermal properties of BisAzo-PC. DSC thermal analysis showed that the pure BisAzo-PC exhibited two endothermic peaks corresponding to the transition temperature T_c and melting temperature T_m at 27.99 °C and 112.04 °C, respectively. The T_c identified here is lower than the *sn-glycero*-3-phosphocholine base lipid.

3.1.3 Photoresponsive properties of BisAzo-PC. The UV-Vis absorption spectra of BisAzo-PC in methanol (0.15 mmol L^{-1}) demonstrated a reduction in the maximum intensity of absorption from 2.75 before irradiation (0 min), to 1.79 after 5 min irradiation, and further down to 1.30 and 1.29 after 10 and 15 min of irradiation, respectively, accompanied by a shift in the maximum absorbance towards 300 nm. This suggests the full conversion from the *trans* to the *cis* isomer is complete within 5 mins of irradiation (Fig. 3(A)), and longer UV exposure times lead to a change in the chemical structure. Conversely, a 120 min relaxation period was required for the maximum absorbance to return to the original intensity, highlighting the ability of BisAzo-PC to rapidly respond to light and isomerize to its *cis* isomer, but a slow reversibility back to its *trans* isomer (Fig. 3(B)). Notably, the maximum absorbance also returns to the original value, indicating that any photodegradation or structural changes were temporary. The repeatability of the reversible photoisomerization of BisAzo-PC was clearly demonstrated by the molecule's ability to return to its original maximum absorbance over ten irradiation-relaxation cycles (10 min photoactivation and 120 min relaxation). The molecule could be switched between the *cis* and *trans* states for three cycles without any measurable change in the maximum absorption intensity. Further cycles stress the molecule and a gradual reduction in the maximum absorption intensity is seen, indicating poor photochemical fatigue and deterioration after numerous cycles (Fig. 3(C)).

3.2 Characteristics of photoresponsive liposomes

Both DPPC-based and HSPC-based photoresponsive liposomes (containing 6% mol BisAzo-PC) produced vesicles of size suitable for dermal delivery. The main characteristics of the liposomes prepared in this study are summarized in Table 1. The hydrodynamic size of both the DPPC and HSPC liposomes post-sonication were comparable at 123.0 and 122.6 nm, respectively. The corresponding zeta potential values were +4.03 and −12.65 mV, respectively, indicating that each formulation possessed a weak surface charge (insufficient for electrostatic repulsive forces to prevent aggregation), which

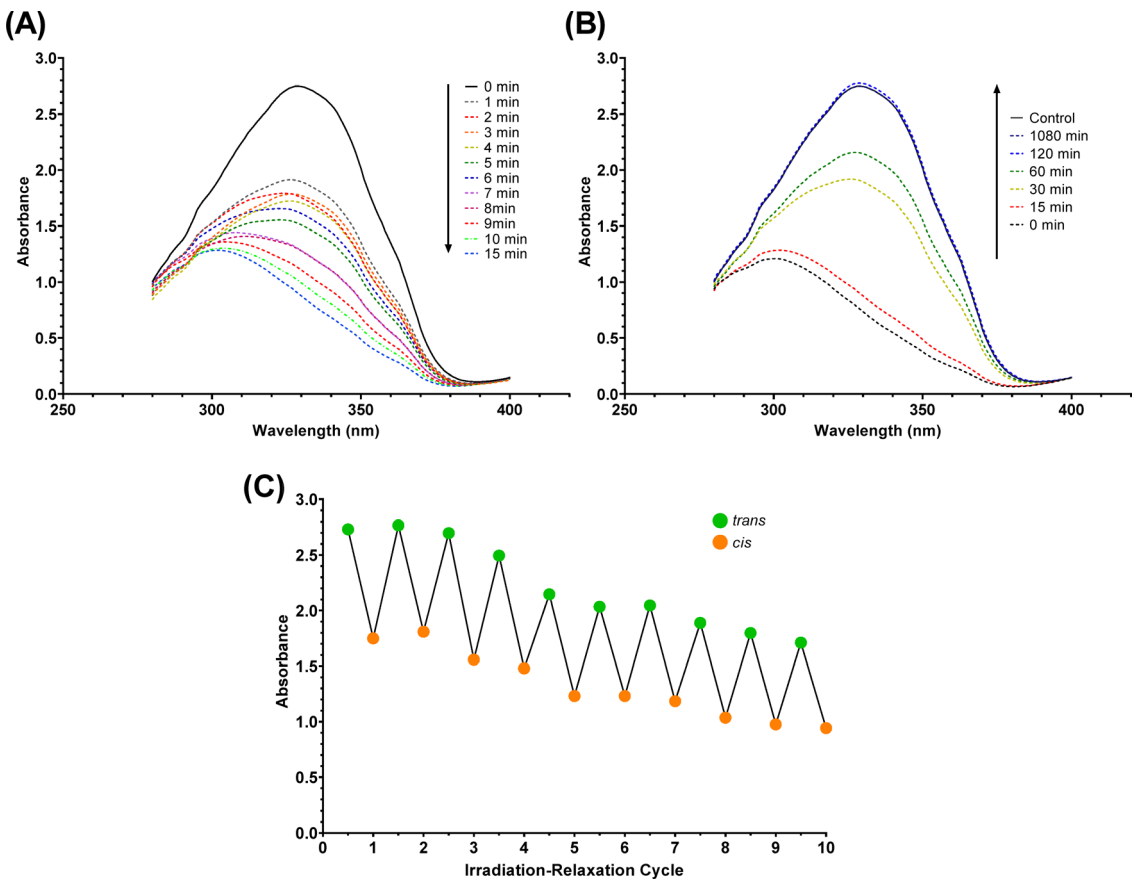

Fig. 3 (A) Photoactivation of BisAzo-PC (*trans* to *cis*) demonstrated by the change in UV-Vis absorbance spectrum before irradiation (0 min) and at each subsequent time point. (B) Relaxation of BisAzo-PC over 18 h after cessation of UV exposure. (C) Multi-switching profile determined by the maximum absorbance of BisAzo-PC for ten cycles (5 min photoactivation and 120 min relaxation) of reversible photoisomerization.

Table 1 Particle size, PDI, zeta potential, UV filter entrapment efficiency (EE) and loading capacity (LC) of conventional non-photosentisive DPPC-based liposomes ($DPPC_{conv}$), and photosensitive DPPC- and HSPC-based liposomes with 6% BisAzo-PC ($DPPC_{ps}$ and $HSPC_{ps}$ respectively). Formulations are co-loaded with benzophenone-4 (BNZ4) and octocrylene (OC). Data are expressed as mean ± SD (n = 3)

Formulation	Z-Ave (nm)	PDI	ZP (mV)	UV Filter	EE (%)	LC (%)
$DPPC_{conv}$	117.2 ± 76.68	0.62 ± 0.06	+5.73 ± 5.49	BNZ4	11.8 ± 2.9	5.6 ± 0.2
				OC	95.2 ± 0.2	9.5 ± 0.1
$DPPC_{ps}$	123.0 ± 29.3	0.53 ± 0.12	+4.03 ± 1.35	BNZ4	25.6 ± 2.2	12.7 ± 0.1
				OC	99.9 ± 0.1	9.9 ± 0.1
$HSPC_{ps}$	122.6 ± 25.5	0.49 ± 0.07	−12.65 ± 0.19	BNZ4	24.8 ± 3.3	12.2 ± 0.8
				OC	99.9 ± 0.1	9.9 ± 0.1

was further reflected in the high PDI values (> 0.2) that indicate a polymodal or a wide size distribution of particles.

The EE and LC of both UV filters were high in both photoresponsive formulations. In particular, the lipophilic octocrylene exhibited a high EE and LC of 99.9% and 9.9% respectively.

3.3 Thermal properties of the liposomal membrane

Next, TGA and DSC data for the DPPC-based and HSPC-based liposomes containing 6% BisAzo-PC were collected. TGA analysis did not show any large changes in sample mass with heating up to 150 °C (Fig. 4), with the small mass loss observed with heating likely due to evaporation of adsorbed water and residual solvents from the purification process. Glass transition temperatures of pure BisAzo-PC the photoresponsive liposomes (containing 6% mol BisAzo-PC) were determined from the DSC curves, with pure BisAzo-PC having a T_c of 27.99 °C, DPPC-based liposomes at 29.42 °C, and the HSPC-based liposomes at 35.93 °C. The melting points were also identified at 112.04 °C, 67.72 °C, and 75.82 °C, respectively.

3.4 Phototriggered UV filter release

The experimental setup is illustrated in Fig. 5(A). Dialysis bags used in the experiments were tested to have a light transmittance of 70% at 365 nm (Fig. 5(B)), indicating its suitability for the subsequent studies. Successful formation of vesicles for DPPC- and HSPC-based photoresponsive liposomes was observed using TEM (Fig. 5(C)) and matched the particle sizes as measured using a Zetasizer.

In all experiments, only benzophenone-4 was detected in the release media. The lipophilic UV filter, octocrylene, had signals below the limit of detection, suggesting that liposomes remained intact and did not break down to release the entrapped lipophilic UV filter from the lipid bilayer.

The cumulative release of benzophenone-4 indicates that DPPC-based liposomes exhibited rapid hydrophilic UV filter leakage across from the aqueous core at all temperatures, and most extensively at the higher temperatures (reaching 100% release after 300 min, Fig. 5(D)-i). Exposure to UV light did not significantly alter the release profiles (Fig. 5(D)-ii). The rapid and complete release of encapsulated benzophenone-4 from the DPPC-based liposomes was likely due to the liposomes being above the T_c, previously determined to be 24.42 °C. As such, the membrane bilayer would be fluid and in a leaky gel phase that was unable to retain the encapsulated payload. In contrast, the HSPC-based liposomes with higher T_c (35.93 °C) retained significantly more benzophophenone-4 at lower temperatures (Fig. 5(E)-i). However, when the temperature was increased above the T_c, rapid and extensive release of benzophophenone-4 was seen with a profile similar to that of the DPPC liposomes. Under continuous exposure to UV light, more benzophenone-4 was released at every point over 360 min compared to the passive release state. Even at temperatures below the T_c (23 and 33 °C), the cumulative release of benzophophenone-4 reached 88.3 ± 3.3% and 87.2 ± 4.2%, respectively (Fig. 5(E)-ii).

The findings suggest that DPPC-based liposomes are not suitable for retaining UV filters for phototriggered release at temperatures below 33 °C, hence would not be applicable for topical applications where the skin has a surface temperature of 33 °C.[39] Alternatively, HSPC-based liposomes demonstrate much less UV filter leakage at temperatures below their T_c.

Phototriggered release studies using either a delayed (after 180 min of passive release) or pulsed UV light were used to evaluate the photoresponsiveness of the liposomes. When delayed UV irradiation was used, the HSPC-based liposomes retained a significant amount of benzophenone-4 over a 180 min period before exposure to light. Immediately after the UV lamp was introduced, a sharp increase in the rate of release was observed (Fig. 6(A)). Similarly, when a pulsed UV irradiation treatment was used (UV lamp irradiation for 15 min after 120 min and 240 min), a sharp increase in the benzophenone-4 release was observed after the first 15 min UV pulse. Following the cessation of UV exposure, the rate of release did not decrease and instead continuously increased linearly. The second UV pulse had no further effect on the benzophenone-4 release rate (Fig. 6(B)). This result corroborates with that of Bisby *et al.*,[13] where the photoisomerization of azobenzenes from *trans* to *cis* isomers was shown to occur rapidly, acting as a rapid 'on' switch, but an extended relaxation time is required for the *cis* isomer to reverse back to the *trans* state, offering a very slow 'off' switch.

3.5 Physical stability

Only HSPC-based liposomes were evaluated for long-term stability trials based on preliminary studies of the thermal properties of the various liposomes (with the DSPC-based liposomes excluded as their glass transition temperature was lower than the surface of the skin, making them wholly suitable for application as a topical sunscreen product).

HSPC-based liposomes were physically stable at both 4 and 25 °C, evidenced by the fact no size change was observed over a

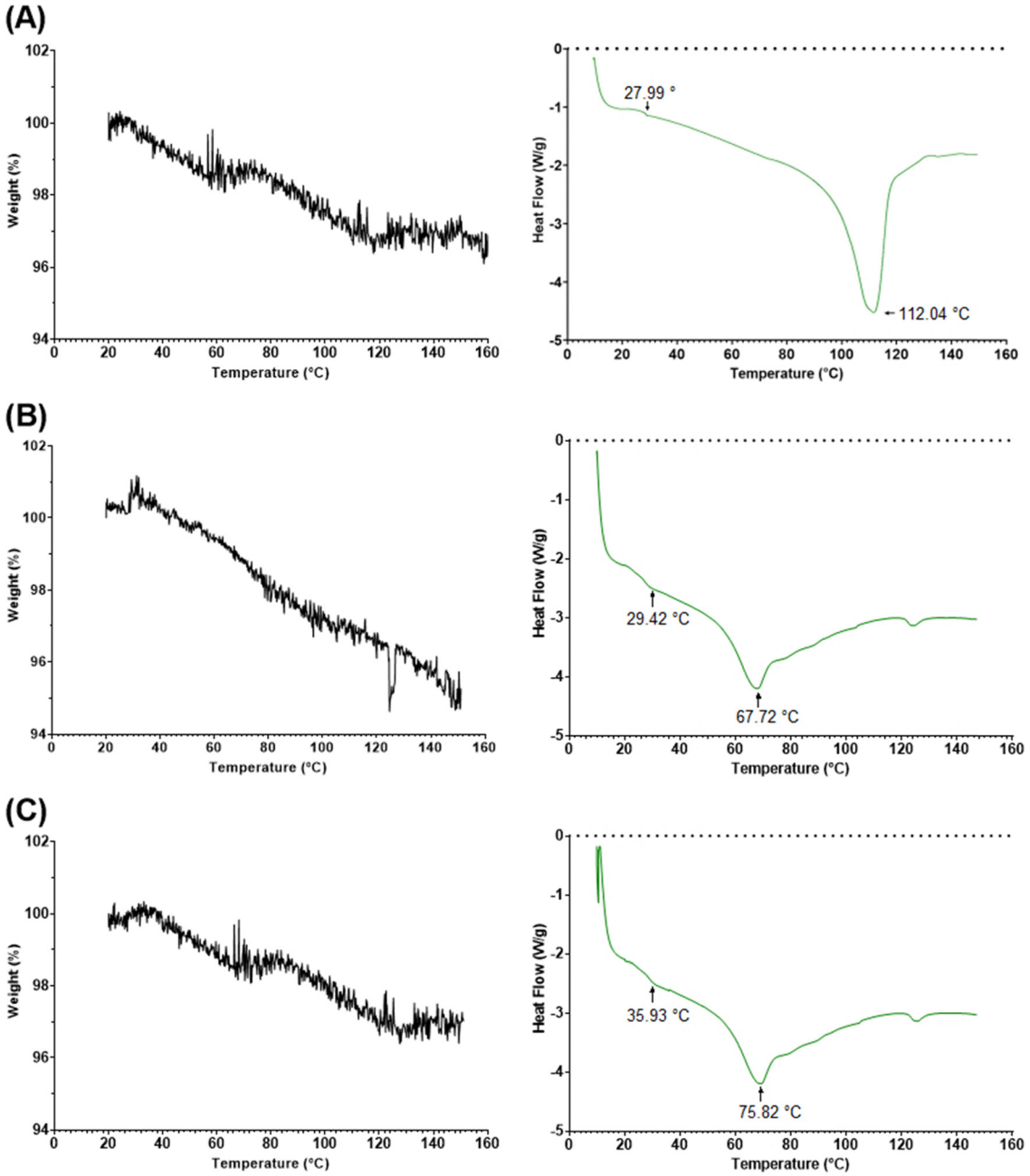

Fig. 4 Thermogravimetric analysis (left) and differential scanning calorimetric curves (right) for (A) pure BisAzo-PC, (B) DPPC-based, and (C) HSPC-based liposomes containing 6% mol BisAzo-PC.

90-day period (Fig. 7). This indicated that the liposomal formulations maintained their integrity and functional characteristics, suggesting they are stable and reliable for extended use. Mild sedimentation without caking was observed and the liposomes could be readily resuspended by inversion. However, with storage at 40 °C (above the T_c), particle size increased rapidly as the liposomal membranes become fluid and destabilized, leading to aggregation and fusion between the lipid particles. Sizes after day 50 could not be determined as the mean particle size was above the measurement range of the Zetasizer instrument.

3.6 Skin permeation, retention, and deposition

3.6.1 Permeation. Permeation studies of the three formulations were conducted using a Franz-Cell diffusion system, with porcine epidermis as the membrane. Benzophenone-4 had a zero-order release profile over 360 min, and octocrylene was not detected in the receptor medium for all samples and formulations.

The liposome formulations in a binary gel were characterized *in vivo* for the skin permeation profile and compared to an equivalent amount of free UV filters in solution as the control. Fig. 8(A) compares the skin permeation profiles of the

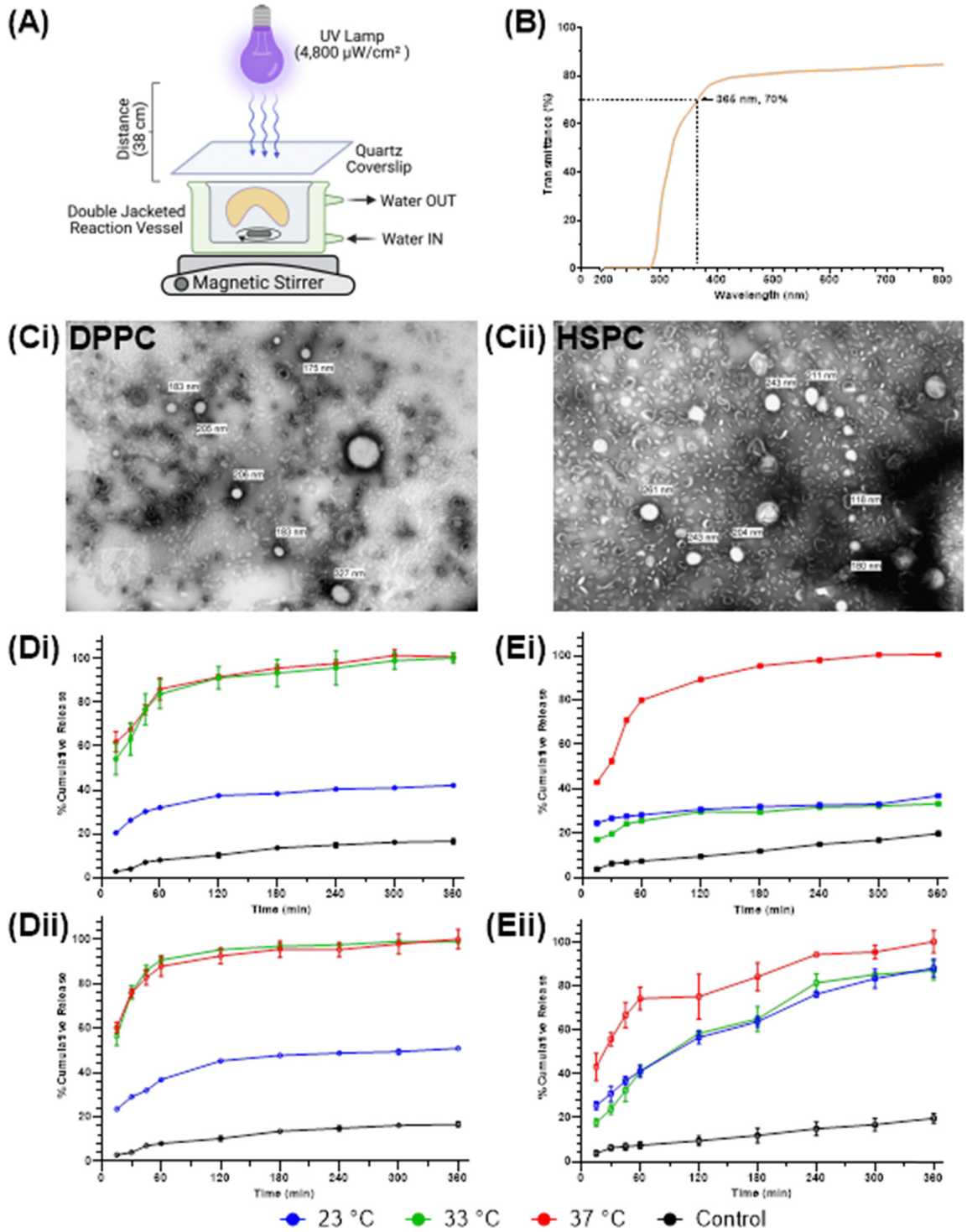

Fig. 5 (A) Experimental setup schematic; (B) UV-Vis spectrum of the dialysis bag showing 70% transmittance at 365 nm; (C) TEM photomicrographs of (i) DPPC- and (ii) HSPC-based photoresponsive liposomes; and (D) and (E) cumulative release profiles of benzophenone-4 from (D) DPPC-based formulations, and (E) HSPC-based formulations; under different light conditions of (i) no light exposure, and (ii) continuous UV light exposure. Control formulations are non-photoresponsive liposomes. Data are mean ± SD (n = 3).

liposome-in-gel formulations to the free drug-gel. The free drug-gel (Free BNZ4 + OC in Gel) had significantly more benzophenone-4 permeated through the epidermis compared to both liposome-in-gel formulation. Non-photoresponsive liposomes (HSPC-Lip$_{conv}$-BAPc0%) had less permeation of benzophenone-4 which could be attributed to the lower amounts of UV filter being released from the liposomes that would be available for permeation. The total amount of benzophenone-4 that permeated through the skin at 360 min was low, with HSPC-Lip$_{conv}$-BAPc0%, HSPC-Lip$_{conv}$-BAPc6%,

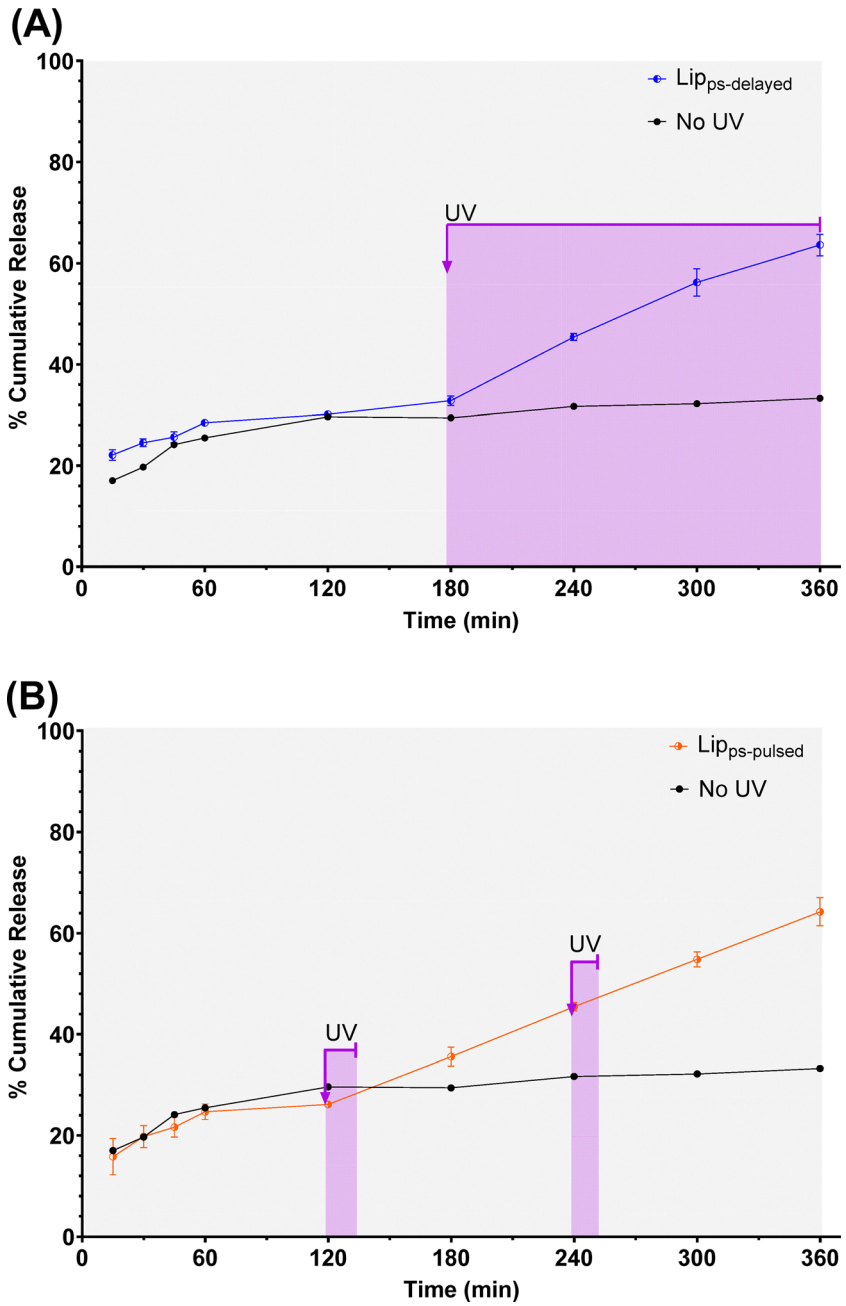

Fig. 6 Cumulative release of benzophenone-4 for (A) delayed, and (B) pulsed UV irradiation patterns of HSPC-based liposomes at 33 °C. UV exposure times are highlighted by the purple regions. Data are mean ± SD (n = 3).

and Free BNZ4 + OC in Gel delivering a total of 1.3%, 1.6%, and 2.1% of the initial dose, respectively.

3.6.2 Retention. Analysis for UV filter content in pulverized tissue after completion of the Franz-Cell permeation study was used to quantify any UV filters retained within the epidermis. From the homogenized tissue we quantify high amounts of the lipophilic octocrylene that was not detected in the receptor medium during permeation studies (Fig. 8(B)), with trace amounts of benzophenone-4.

3.6.3 Deposition. Analysis of tape strippings from full-thickness skin to determine the deposition of both benzophenone-4 and octocrylene in the first twelve layers of the stratum corneum (Fig. 9). The optimized photoresponsive liposome-in-gel formulation showed a constant concentration of benzophenone-4 throughout the stratum corneum layers, indicative of a rapid but consistent penetration of the liposomes through the stratum corneum into the layers below, possibly through both the transcellular and paracellular pathways.[40] Conversely, octocrylene had a more gradual penetration profile, with the majority of UV filter limited to the first three layers of the stratum corneum. This suggests that the liposomes may accumulate on the first few layers of the stratum corneum, where hydrophilic

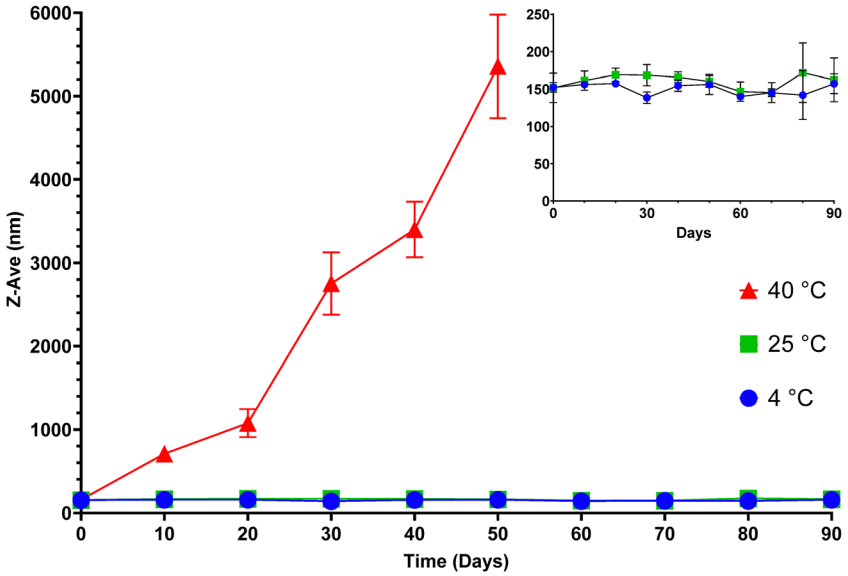

Fig. 7 Long-term physical stability of HSPC-based liposomes at 4, 25, and 40 °C. Liposome sizes are expressed as mean ± SD (n = 3). Inset: Zoomed in y-axis, noting no size change over 90 days at 4 and 25 °C.

benzophenone-4 could diffuse rapidly through the cells, and lipophilic octocrylene would localize and diffuse out slowly.

3.7 Cellular response to UV light and photoprotective effects of photoresponsive liposome-in-gel

3.7.1 Cell viability and morphology. The viability of cells as determined by the CCK8 assay when fully exposed to UV light exhibited an increasing loss of viability with longer UV exposure times. Exposure times of up to 5 min did not significantly cause a loss of viability immediately or 24 h after irradiation. However, once exposed for 10 min, significant cell death was immediately seen, with cell viability decreasing by 8.3% and further by 53.2% after 24 h (Fig. 10(A)). More extensive loss in cell viability is seen with longer UV exposure times, highlighting a lag time before cell death occurs. Subsequent experiments had a UV exposure time of 10 min to ensure maximal response of ROS generation, with a modest loss of cell viability so protective effects of the formulations can be examined. Immediate cell death was prevented when cells were protected by either *Cicatricure* (a commercial sunscreen) or Gel + Lip_{ps} + drug, demonstrating the photoprotective properties of the formulations. Furthermore, no significant loss of cell viability was seen after 24 h post irradiation for both formulations (Fig. 10(B)).

3.7.2 Intracellular ROS generation. During the 6 h experiment, the cells without UV exposure had a small but gradual increase in RFU from 1.0 to 1.2 whereas the cells with full UV exposure had a RFU of 22.2, suggesting high production of ROS upon UV light exposure. The liposome-in-gel formulation (Gel + Lip_{ps} + drug) had 72% less RFU than that of fully exposed cells. Notably, in comparison to the commercial sunscreen (*Cicatricure*), Gel + Lip_{ps} + drug had 15% reduction in RFU after 6 h (Fig. 11), demonstrating that the photoresponsive liposomes

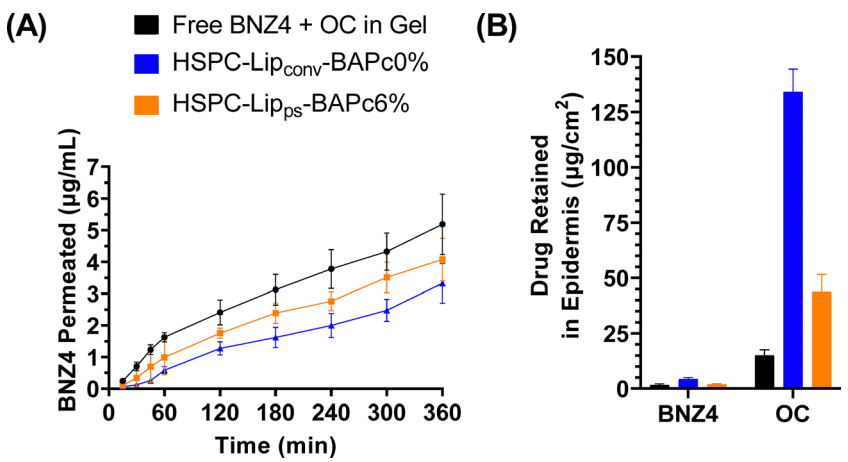

Fig. 8 (A) Skin permeation of benzophenone-4 (BNZ4). (B) UV filter retention in the epidermis of BNZ4 and octocrylene (OC).

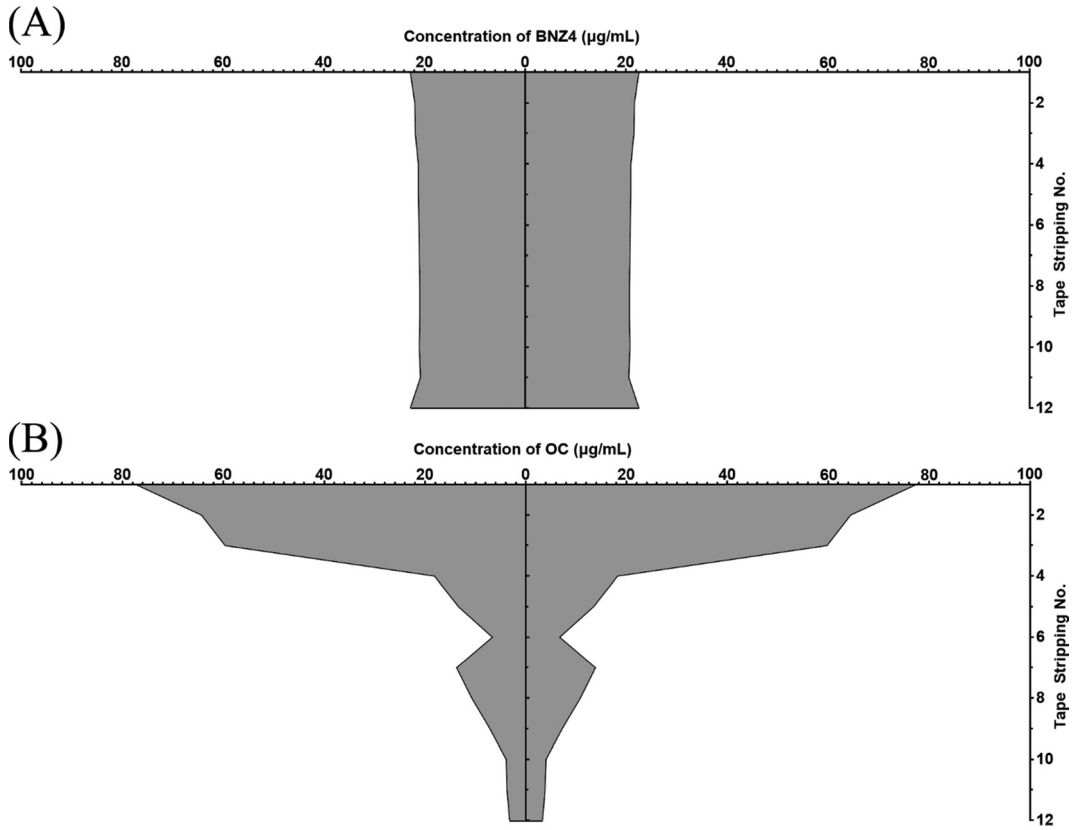

Fig. 9 UV filter deposition profile of (A) benzophenone-4 (BNZ) and (B) octocrylene (OC), in the stratum corneum by liposome-in-gel (HSPC-based photoresponsive liposomes; (HSPC:Chol:BisAzo-PC; 84, 10, 6 mol%) in H12P6 gel; 50/50 w/w) as determined by tape stripping.

had a greater ability to protect the HDFn cells from UV induced ROS generation. Furthermore, the H12P6 binary gel itself (Gel) had a RFU of 5.4, indicating that the blank gel alone had a degree of photoprotection. Gel + Lip_{conv} and Gel + Lip_{ps} had higher than expected RFU values above Gel alone and is likely due to the dilution of the matrix upon addition of the liposomal suspension.

3.7.3 Oxidative stress markers

Lipid peroxidation. The MDA assay revealed extensive lipid peroxidation in the cells after UV exposure (10 min) in all

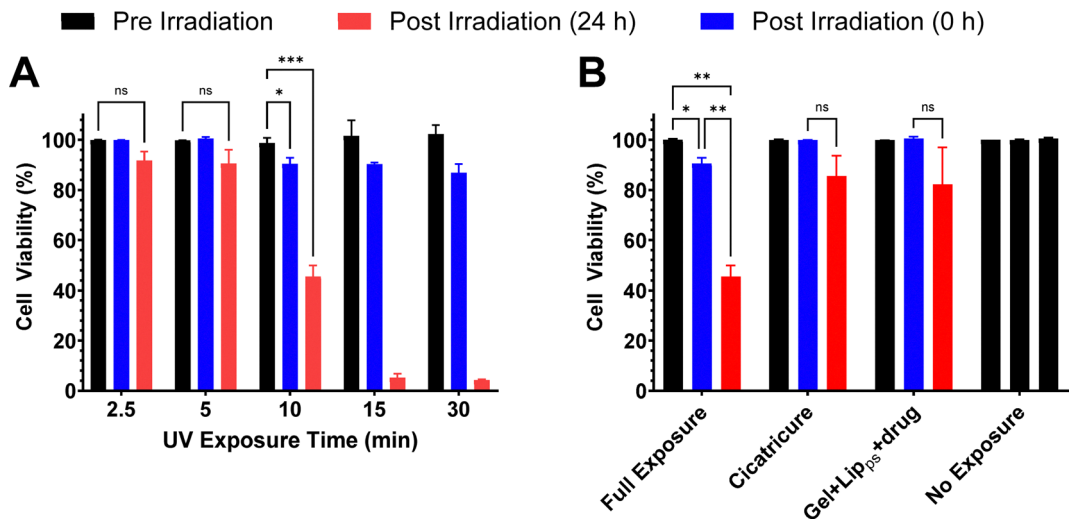

Fig. 10 (A) Cell viability of HDFn cells after exposure to varying lengths of UV light. (B) Acute protective effects of *Cicatricure* and photoresponsive liposomes in gel (Gel + Lip_{ps} + drug) in HDFn cells after UV exposure (10 min). Cell viability was measured using the Cell Counting Kit-8 Assay. Data are mean ± SD (n = 3). *: $p < 0.05$; ***: $p < 0.001$; ns = non-significant difference.

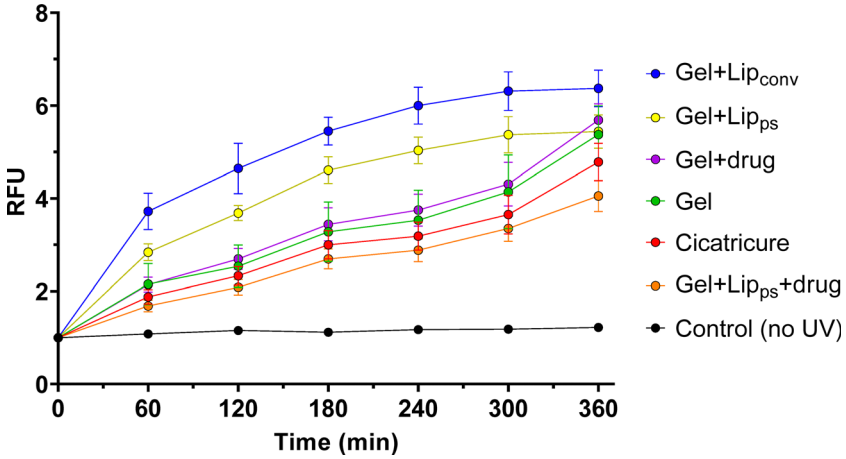

Fig. 11 UV protection of formulations measured as the total intracellular ROS levels of HDFn, expressed as Relative Fluorescence Units (RFU) to the cells with full UV exposure. Data are mean ± SD (n = 3).

formulations. Full UV exposure caused a 7-fold increase in cellular MDA concentrations ($p < 0.001$) (Fig. 12(A)), indicating the strong oxidizing effect of UV light on the HDFn cells and the resulting damage to the lipid membrane. All formulations resulted in significantly decreased MDA concentrations compared to fully exposed cells, indicating the photoprotective effect against oxidation induced by UV light. Significant protection ($p < 0.05$) was found for both *Cicatricure* Gel and Gel + Lip_{ps} + drug formulations, with no significant difference identified between the two, indicating that Gel + Lip_{ps} + drug has a comparable protection effect against lipid peroxidation as the commercial product.

Antioxidant enzyme activities. SOD enzyme activity was upregulated by all formulations and cells that are exposed to UV irradiation, though cells treated with the formulations showed significantly less SOD enzyme activity than fully exposed cells, indicating less intracellular oxidative stress due to the photoprotection provided by these formulations. However, no statistically significant difference was found between all formulations (Fig. 12(B)).

GPx enzyme activity was expected to decrease in response to significant lipid peroxidation of the cell membrane as the enzyme is depleted to remove the free peroxide in the cell. This effect was seen between the control groups of full and no exposure to UV light. Photoprotection of the cells with formulations generally increased the activity of GPx, indicating that less oxidative damage has occurred within the cell. GPx was significantly depleted across all groups after UV irradiation, with *Cicatricure* and Gel + Lip_{ps} + drug formulations having no significant difference in GPx activity (Fig. 12(C)).

3.8 Universal sun protection factor

The UV-Vis spectra of each formulation were analysed and the uSPF values are summarized in Table 2. A uSPF value of 8.2 ± 1.3 was observed in the H12P6 binary gel alone (Gel), corroborating with the previous results of the intracellular ROS generation over time that suggested the gel alone provided a degree of protection against UV light. The photoresponsive liposome loaded with UV filters was the most protective at uSPF 38.1 ± 1.1, followed by the commercial sunscreen, *Cicatricure* at 32.3 ± 0.1 which also meets the label claim of 30 SPF. All other formulations had a modest uSPF value.

4. Discussion

Photoresponsive liposome delivery systems attract great interest due to their high spatial and temporal precision as a means of regulating drug release. The addition of a photoresponsive lipid such as BisAzo-PC into the liposomal membrane allows for phototriggered release of encapsulated drug (UV filters in this case), however, it is important to understand how such photosensitizers affect membrane stability.

The photoresponsive studies demonstrate the overall photoresponsive properties of BisAzo-PC, with results suggesting that it can rapidly photoisomerize and will have the capability to quickly induce membrane destabilization and thus drug release. Photoresponsive studies demonstrated a UV irradiation (365 nm) time of 5 min is required to induce isomerisation to the *cis* isomer, and longer exposure time leads to a shift in the maximum absorbance. This shift suggests that photolysis of BisAzo-PC has occurred, resulting in the enhancement of weak n → π* transitions responsible for visible absorption, accompanied with a shift to the shorter wavelength of the main π–π* transition. However, full recovery of the spectra is observed after a 2 h relaxation period, suggesting reversible mechanisms other than photolysis is involved, and further investigation into the photochemical and structural properties of BisAzo-PC is warranted. Repeated photoactivation and relaxation cycles indicate a relatively poor photochemical fatigue resistance, and it does not detract from the application in a sunscreen where there will be a limited number of cycles. However, the molecule required significantly more time (2 h) to reverse back to its initial stable *trans* isomer, implying that BisAzo-PC is not the most suitable photo-switch when designed for an

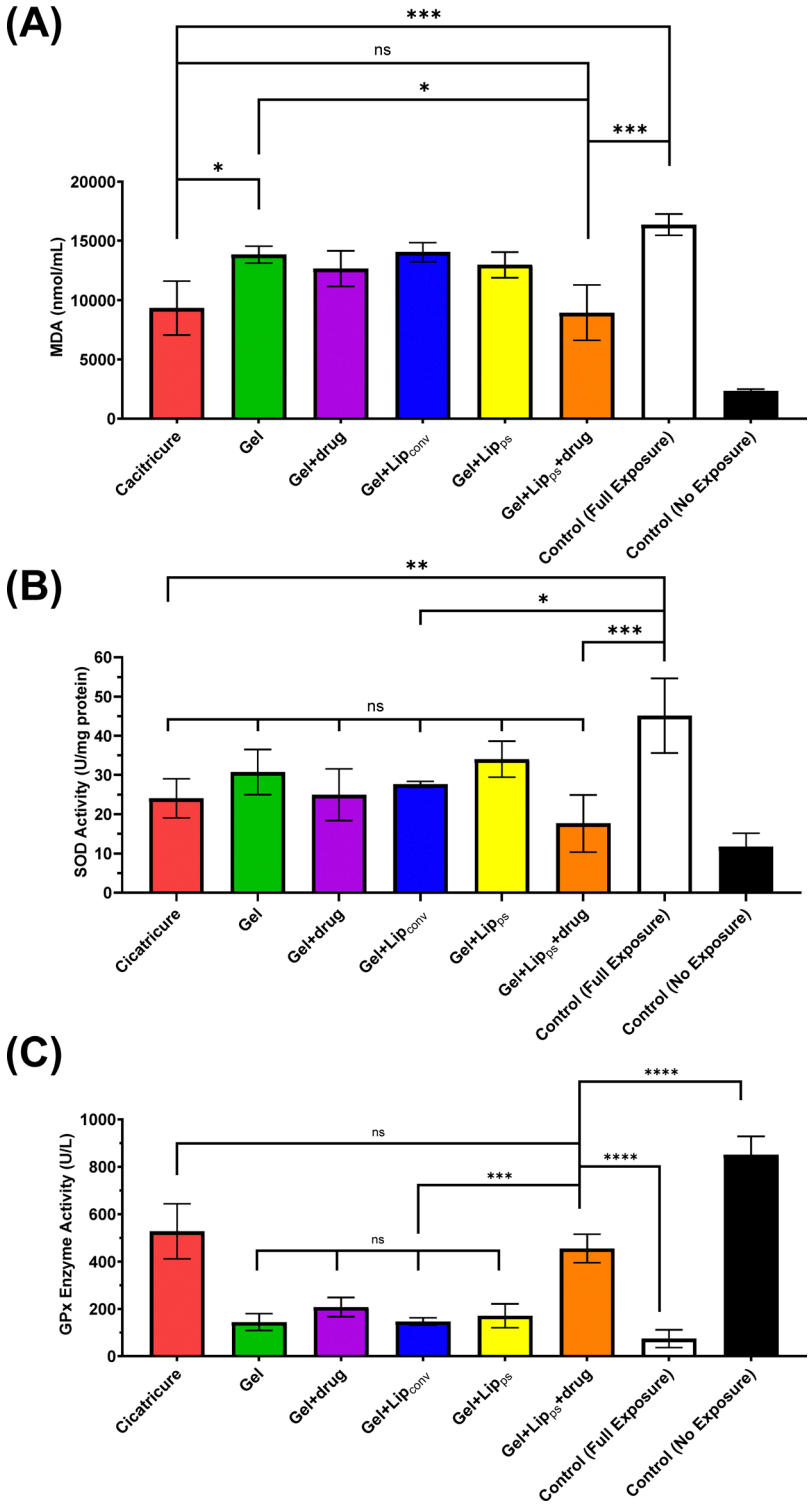

Fig. 12 Effect of UV exposure (10 min) on HDFn cells protected by various formulations and the resulting: (A) malondialdehyde (MDA) concentrations, indicative of the degree of oxidative damage in the cell membrane, (B) superoxide dismutase (SOD) enzyme activity; and (C) glutathione peroxidase (GPx) enzyme activity. Data are mean ± SD (n = 3). *: $p \leq 0.05$; **: $p \leq 0.01$; ***: $p \leq 0.001$; ns = non-significant.

application such as a sunscreen where shorter time periods will be required to obtain a true ''on–off'' drug release switch.

Both photoresponsive DPPC and HSPC-based liposomes could easily attain the optimal particle sizes between 100–600 nm for dermal delivery using the thin-film hydration method with brief sonication.[41] A very high EE of 99% for the lipophilic octocrylene was achieved, but not for the hydrophilic benzophenone-4. This is in-line with literature where lipophilic

Table 2 Summary of the calculated uSPF values for each formulation. Data are mean ± SD (n = 3)

Formulation	uSPF
Cicatricure	32.3 ± 0.1
Gel	8.2 ± 1.3
Gel + Drug	8.2 ± 0.9
Gel + Lip_{ps} + Drug	38.1 ± 1.1
Gel + Lip_{conv}	6.6 ± 0.8
Gel + Lip_{ps}	7.2 ± 0.8

compounds are easily incorporated into lipid bilayer membranes, and was seen for other lipophilic UV filters such as octyl methoxycinnamate.[42,43] Hydrophilic compounds are entrapped in the aqueous core of the vesicles and their concentration is limited by the solubility of the compound and the volume of the aqueous core, with any improvements in uptake requiring alternate drug loading techniques such as active loading.

The thermal properties of liposomes play a crucial role in their functional characteristics, including membrane stability. The T_c is a key element when examining membrane stability of liposomes, and it is defined as the temperature required to induce a change in the physical state of the lipid from the ordered gel phase to the disordered liquid-crystalline phase. Consequentially, when liposomes are above their T_c, the fluid membrane is less able to retain the encapsulated contents. In this study, this was observed in both the long-term stability profiles of the liposomes as well as in phototriggered drug release studies, where rapid and extensive leakage of hydrophilic drug is seen. Simultaneously, no release of lipophilic drug was observed even when at temperatures above T_c, suggesting that the lipid membrane remains intact. HSPC-based liposomes had a higher T_c and are considered more thermodynamically stable than those prepared with DPPC. The membrane stability, and thus, capacity to retain drug is seen in the phototriggered drug release profiles at different temperatures where all formulations at high temperatures above their respective T_c experienced rapid and extensive drug release. However, BisAzo-PC had a measured T_c of 27.99 °C, conflicting with a previously reported value of 41 °C by Morgan *et al.*[44] that concluded that the presence of the N=N within the hydrocarbon chain of the lipid does not impact thermal stability. In this study, DSC thermograms of pure, freshly synthesized BisAzo-PC (structurally confirmed by FTIR, LC–MS, and ^{1}H NMR) clearly identified a much lower T_c. This suggests that the N=N azo functional group has a destabilising effect regarding the thermal stability of the compound. With consideration of these results, we postulate that, as the chemical structure of BisAzo-PC indicates no intramolecular hydrogen bonding is possible, it has poor capacity to maintain a high thermal stability at the N=N diazenyl bond.[45] Furthermore, thermal *cis–trans* isomerization follows an inversion mechanism,[46] and along with existing ring strain within the *trans–cis* isomer, a lower degree of thermal stability is expected.[47]

The phototriggered drug release properties provided by BisAzo-PC is highly responsive to UV light (365 nm), with photoresponsive liposome formulations achieving a high drug release of more than 80%, while also providing a relatively slow rate of release over 6 h. In comparison, research conducted by Enzian *et al.*[17] investigated the use of four different photosensitisers (BPD, $AlPcS_2$, Ce6, and 5,10-DiOH) to impart photosensitivity to the liposomes, and drug release was complete (100%) within 10 min of irradiation for all formulations. In contrast, Shen *et al.* prepared photoresponsive micelles using a photoresponsive spiropyran block copolymer, achieving a much lower drug release of 50% doxorubicin after 24 h.[48] While azobenzene-based compounds remain one of the most popular methods for imparting photoresponsive properties to drug delivery systems due to their reversible *cis–trans* photoisomerization,[49] BisAzo-PC liposomes have been poorly investigated, with only five studies known to date.[11,12,15,16,44] This study demonstrates a photoresponsive liposome and its suitability in applications where phototriggered release for delivery of ~6 hours is desired. However, due to BisAzo-PC's rapid initiation and slow reversal, the present formulation is not applicable to clinical situations that require multi-pulsatile release. Further optimisation of the formulation could extend the drug release capabilities to different controlled release requirements. The effects of photothermal heating on the liposomes when exposed to long durations of UV light also need to be considered in the interpretation of the results. In particular, the relatively low T_c of both DPPC- and HSPC-based liposomes could lead to increased membrane instability and increased leakage of the encapsulated cargo. Improvement of the experimental setup to monitor the temperature of both the external media as well as the liposomes within the dialysis bags, such as with a thermal imaging camera, will offer valuable insight into the effect and significance of photothermal heating on drug release.

Skin permeation and retention studies on excised porcine epidermis found that only hydrophilic benzophenone-4 penetrated through the epidermis, while lipophilic octocrylene was localized in the, a relatively large amount of octocrylene was detected. This data, paired with the skin deposition profiles investigated using the tape stripping method suggests that the liposomes accumulated in the top layers of the stratum corneum where octocrylene is slowly released as the liposome degrades. In contrast, benzophenone-4 could be detected in both the stratum corneum and epidermis, while also being able to permeate through the epidermis into the receptor medium of the Franz-Cell study. This is likely explained by the ability of hydrophilic drugs to penetrate *via* the transcellular pathway.[50] The skin permeation, retention, and deposition study results indicate that only small amounts of the UV filters, benzophenone-4 and octocrylene, would have the potential to penetrate the skin and be absorbed systemically to exert toxic effects.[50] Other factors not controlled for could also influence the percutaneous absorption of drug through the skin. The hydration of the skin is one other example where large differences in drug absorption could be observed.[50] The greater the hydration, the higher the absorption of substances, particularly hydrophilic molecules. High skin hydration is the result of the accumulation of water when a barrier or other occlusive vehicle

is applied over the skin, and the binary gel used to suspend the liposome could potentially affect this. Other factors to consider include the area and method, region, period of application, the age of the skin, and the use of vehicles which alter barrier function or improve bioadhesiveness, would need to be considered carefully to achieve a useable product.

By investigating the amount of ROS generated when HDFn cells were exposed to various doses of UV light, an UV irradiation time of 5 min was established to be sufficient in eliciting the maximum response from the cells for the generation of ROS, and implicitly, the amount of damage that could potentially be induced on the cell before significant cell death. The results from the ROS generation of time studies, alongside the measured uSPF values of each formulation indicate that all formulations offered a strong degree of UV protection, compared to cells fully exposed to UV light. Notably, the ranked order of protection (as identified by the uSPF values), broadly matched the order also seen in the ROS generation of time studies. The photoresponsive liposome-in-gel formulation had the greatest uSPF value, which also had the lowest RFU at 6 h, indicating that the developed formulation had greater photoprotective effects than the commercial sunscreen, *Cicatricure*. Furthermore, H12P6 binary gel (with no UV filters) demonstrated a small degree of photoprotection, having a measured uSPF value of 8.2 ± 1.3, which has not been previously reported in the literature. This could be due to PVP, which contains a pyrrolidine cyclic secondary amine within its chemical structure and exhibits light absorbance properties due to its electron-donor effect. This finding is of great interest for developing topical sunscreen bases where UV absorbance is desirable, as it allows for additional UV light protection without adding extra UV filters that could be systemically absorbed and lead to toxicity, and have maximum limits set by regulatory bodies. Further investigation is required to determine the degree of photoprotection provided solely by the binary gel, and may be of particular interest in further development of an improved sunscreen base.

Evaluation of oxidative stress markers such as MDA and the antioxidant activities of SOD and GPx indicated that *Cicatricure* and Gel + Lip_{ps} + drug formulations could significantly reduce intracellular oxidative stress and potentially aid in preventing lipid oxidation. MDA, which is one of the toxic end-products of the lipid peroxidation process when ROS react with polyunsaturated fatty acids, is generally indicative of cell damage caused by free radicals.[51] This chemical process is immediate and as such, the results reflect the rapid and significant changes in MDA levels between the formulations after UV exposure. Antioxidant enzyme activities also demonstrated significant differences when compared to unprotected cells. However, we note that due to the short period between UV irradiation and the assays, there may be insufficient time for the cells to upregulate the amount of SOD and GPx enzymes to achieve their highest antioxidant enzyme concentrations. One study performed by Nethravathy *et al.* measured SOD production over time in a *Saccharomyces mellis* yeast model and demonstrated that at least 48 h is required for SOD activity to reach its maximum.[52] The depletion of GPx *vs* time required for maximum SOD and GPx enzyme responses will need to be optimized for each experimental condition and cell line in order to achieve the best responses for analysis.

As studies were performed on an *in vitro* model with isolated HDFn cells, which do not mimic *in vivo* conditions where the skin presents itself in multiple layers with various components alongside other cells, such as melanocytes that produce photoprotective melanin, the thickness of the overlying epidermis, and other active DNA repair pathways such as base and nucleotide excision repair. A more comprehensive investigation should be performed using *in vivo* models where all other components of the skin are present to provide a full picture of the biochemical responses.

5. Conclusion

Photoresponsive liposomes were developed and incorporated into a binary gel formulation, providing a high degree of photoprotection as is evident by the high uSPF, reduction in intracellular ROS and lipid peroxidation levels, and changes in antioxidant enzyme expression in HDFs when protected by the formulation after exposure to UV light. Cell viability can be maintained by protecting the cells from UV light with the developed Gel + Lip_{ps} + drug formulation. A lag time in cell death, observed 24 h after UV irradiation, suggests that the damage induced by UV light – whether directly on the DNA or mediated by other downstream effects such as by ROS, requires additional methods such as an *in vivo* animal model to fully analyse the formulations. Despite the photoresponsive lipid not being able to achieve a multi-pulsatile release for UV filter delivery, the overall results suggest that a photoresponsive liposome-in-gel formulation had greater UV protection than a commercial sunscreen and has potential for extending the UV protection provided by traditional sunscreen formulations.

Conflicts of interest

There are no conflicts to declare.

Data availability

The data supporting this article have been included within the article or as part of the SI (including chemical synthesis experimental procedures, NMR, and MS spectrums). See DOI: **https://doi.org/10.1039/d5ma00460h**.

Acknowledgements

The authors wish to acknowledge Patrick Pan's University Doctoral Scholarship from the University of Auckland. We would like to gratefully acknowledge Dr Irene Jeongin Kim from the School of Chemical Sciences at the University of Auckland for their assistance in chemical schematic drawing, NMR and MS data interpretation. We also thank Ms Jacqueline

Ross and the Biomedical Imaging Research Unit (BIRU) at the University of Auckland for their support in acquiring TEM photomicrographs.

References

1 A. H. Roky, M. M. Islam, A. M. F. Ahasan, M. S. Mostaq, M. Z. Mahmud and M. N. Amin, *et al.*, Overview of skin cancer types and prevalence rates across continents, *Cancer Pathog. Ther.*, 2024, **3**(2), 89–100.
2 M. R. Wehner, Sunscreen and melanoma prevention: evidence and expectations, *Br. J. Dermatol.*, 2018, **178**(1), 15.
3 M. Sander, M. Sander, T. Burbidge and J. Beecker, The efficacy and safety of sunscreen use for the prevention of skin cancer, *Can. Med. Assoc. J.*, 2020, **192**(50), E1802.
4 R. Lapides, B. Saravi, A. Mueller, M. Wang-Evers, L. V. Maul and I. Németh, *et al.*, Possible Explanations for Rising Melanoma Rates Despite Increased Sunscreen Use over the Past Several Decades, *Cancers*, 2023, **15**(24), 5868.
5 M. K. Matta, J. Florian, R. Zusterzeel, N. R. Pilli, V. Patel and D. A. Volpe, *et al.*, Effect of Sunscreen Application on Plasma Concentration of Sunscreen Active Ingredients: A Randomized Clinical Trial, *JAMA*, 2020, **323**(3), 256–267.
6 V. Mustieles, R. K. Balogh, M. Axelstad, P. Montazeri, S. Márquez and M. Vrijheid, *et al.*, Benzophenone-3: Comprehensive review of the toxicological and human evidence with meta-analysis of human biomonitoring studies, *Environ. Int.*, 2023, **173**, 107739.
7 W. Kobwanthanakun, N. Silpa-archa, C. Wongpraparut, C. Pruksaekanan and W. Manuskiatti, An evaluation of the course of facial sunscreen coverage and sustainability over an 8-hour workday among outdoor workers, *Health Sci. Rep.*, 2021, **4**(3), e350.
8 M. F. Peralta, M. L. Guzmán, A. P. Pérez, G. A. Apezteguia, M. L. Fórmica and E. L. Romero, *et al.*, Liposomes can both enhance or reduce drugs penetration through the skin, *Sci. Rep.*, 2018, **8**, 13253.
9 P. Pan, D. Svirskis, S. W. P. Rees, D. Barker, G. I. N. Waterhouse and Z. Wu, Photosensitive drug delivery systems for cancer therapy: Mechanisms and applications, *J. Controlled Release*, 2021, **338**, 446–461.
10 S. Sun, S. Liang, W. C. Xu, G. Xu and S. Wu, Photoresponsive polymers with multi-azobenzene groups, *Polym. Chem.*, 2019, **10**(32), 4389–4401.
11 R. H. Bisby, C. Mead and C. G. Morgan, Photosensitive liposomes as ''cages'' for laser-triggered solute delivery: the effect of bilayer cholesterol on kinetics of solute release, *FEBS Lett.*, 1999, **463**(1–2), 165–168.
12 C. G. Morgan, Y. P. Yianni, S. S. Sandhu and A. C. Mitchell, Liposome fusion and lipid exchange on ultraviolet irradiation of liposomes containing a photochromic phospholipid, *Photochem. Photobiol.*, 1995, **62**(1), 24–29.
13 R. H. Bisby, C. Mead, A. C. Mitchell and C. G. Morgan, Fast Laser-Induced Solute Release from Liposomes Sensitized with Photochromic Lipid: Effects of Temperature, Lipid Host, and Sensitizer Concentration, *Biochem. Biophys. Res. Commun.*, 1999, **262**(2), 406–410.
14 R. H. Bisby, C. Mead and C. G. Morgan, Active uptake of drugs into photosensitive liposomes and rapid release on UV photolysis, *Photochem. Photobiol.*, 2000, **72**(1), 57–61.
15 S. D. Pritzl, J. Morstein, S. Kahler, D. B. Konrad, D. Trauner and T. Lohmüller, Postsynthetic Photocontrol of Giant Liposomes *via* Fusion-Based Photolipid Doping, *Langmuir*, 2022, **38**(39), 11941–11949.
16 C. G. Morgan, E. W. Thomas, S. S. Sandhu, Y. P. Yianni and A. C. Mitchell, Light-induced fusion of liposomes with release of trapped marker dye is sensitised by photochromic phospholipid, *Biochim. Biophys. Acta*, 1987, **903**(3), 504–509.
17 P. Enzian, C. Schell, A. Link, C. Malich, R. Pries and B. Wollenberg, *et al.*, Optically Controlled Drug Release from Light-Sensitive Liposomes with the New Photosensitizer 5,10-DiOH, *Mol. Pharmaceutics*, 2020, **17**(8), 2779–2788.
18 M. Tang, S. B. Yarragudi, P. Pan, K. Yang, M. Kanamala and Z. Wu, Effect of size and pH-sensitivity of liposomes on cellular uptake pathways and pharmacokinetics of encapsulated gemcitabine, *J. Liposome Res.*, 2024, 1–11.
19 H. Xu, J. Paxton, J. Lim, Y. Li and Z. Wu, Development of a gradient high performance liquid chromatography assay for simultaneous analysis of hydrophilic gemcitabine and lipophilic curcumin using a central composite design and its application in liposome development, *J. Pharm. Biomed. Anal.*, 2014, **98**, 371–378.
20 M. Kamra, A. Diwan and S. Sardana, Topical Liposomeal Gel: A Review, *Int. J. Pharma Sci. Res.*, 2017, **8**(6), 2408–2414.
21 Y. Mou, P. Zhang, W. F. Lai and D. Zhang, Design and applications of liposome-in-gel as carriers for cancer therapy, *Drug Delivery*, 2022, **29**(1), 3245.
22 P. Pan, D. Svirskis, G. I. N. Waterhouse and Z. Wu, Hydroxypropyl Methylcellulose Bioadhesive Hydrogels for Topical Application and Sustained Drug Release: The Effect of Polyvinylpyrrolidone on the Physicomechanical Properties of Hydrogel, *Pharmaceutics*, 2023, **15**(9), 2360.
23 W. Gao, D. Vecchio, J. Li, J. Zhu, Q. Zhang and V. Fu, *et al.*, Hydrogel Containing Nanoparticle-Stabilized Liposomes for Topical Antimicrobial Delivery, *ACS Nano*, 2014, **8**(3), 2900–2907.
24 R. Binaymotlagh, F. H. Haghighi, L. Chronopoulou and C. Palocci, Liposome–Hydrogel Composites for Controlled Drug Delivery Applications, *Gels*, 2024, **10**(4), 284.
25 R. J. Kennedy and A. M. Stock, The Oxidation of Organic Substances by Potassium Peroxymonosulfate, *J. Org. Chem.*, 1960, **25**(11), 1901–1906.
26 S. S. Sandhu, Y. P. Yianni, C. G. Morgan, D. M. Taylor and B. Zaba, The formation and Langmuir-Blodgett deposition of monolayers of novel photochromic azobenzene-containing phospholipid molecules, *Biochim. Biophys. Acta, Biomembr.*, 1986, **860**(2), 253–262.
27 I. J. Kim, L. I. Pilkington and D. Barker, Total Synthesis of (−)-Amovillosumin A and Structure Correction of (−)-Amovillosumin C Using Chemical Synthesis, *J. Nat. Prod.*, 2024, **87**(2), 340–348.

28 I. J. Kim, L. I. Pilkington and D. Barker, Total Synthesis of Linear Coumarniolignoids (+) and (−)-Sapiumin C, (−)-Moluccanin, and (−)-Hemidesminine, *J. Org. Chem.*, 2023, **88**(9), 5900–5912.
29 P. Pan, D. Svirskis, G. I. N. Waterhouse and Z. Wu, A simple and reliable isocratic high-performance chromatographic assay for the simultaneous determination of hydrophilic benzophenone-4 and lipophilic octocrylene in sunscreens, *Int. J. Cosmet. Sci.*, 2023, **45**(4), 512–523.
30 L. Jian, Y. Cao and Y. Zou, Dermal-Epidermal Separation by Heat, in *Epidermal Cells: Methods and Protocols*, ed. K. Turksen, Springer, New York, NY, US, 2020, pp. 23–25.
31 D. J. Davies, R. J. Ward and J. R. Heylings, Multi-species assessment of electrical resistance as a skin integrity marker for *in vitro* percutaneous absorption studies, *Toxicol. In Vitro*, 2004, **18**(3), 351–358.
32 Test No. 428: Skin Absorption: *In Vitro* Method, OECD Guidelines for the Test of Chemicals, Section 4. OECD. 2004.
33 A. Ayala, M. F. Muñoz and S. Argüelles, Lipid Peroxidation: Production, Metabolism, and Signaling Mechanisms of Malondialdehyde and 4-Hydroxy-2-Nonenal, *Oxid. Med. Cell. Longevity*, 2014, **2014**, 360438.
34 N. S. Aliahmat, M. R. M. Noor, W. J. W. Yusof, S. Makpol, W. Z. W. Ngah and Y. A. M. Yusof, Antioxidant enzyme activity and malondialdehyde levels can be modulated by Piper betle, tocotrienol rich fraction and Chlorella vulgaris in aging C57BL/6 mice, *Clinics*, 2012, **67**(12), 1447.
35 O. M. Ighodaro and O. A. Akinloye, First line defence antioxidants-superoxide dismutase (SOD), catalase (CAT) and glutathione peroxidase (GPX): Their fundamental role in the entire antioxidant defence grid, *Alex J Med.*, 2018, **54**(4), 287–293.
36 A. V. Peskin and C. C. Winterbourn, Assay of superoxide dismutase activity in a plate assay using WST-1, *Free Radical Biol. Med.*, 2017, **103**, 188–191.
37 A. Bizoń, J. Chojdak-Łukasiewicz, S. Budrewicz, A. Pokryszko-Dragan and A. Piwowar, Exploring the Relationship between Antioxidant Enzymes, Oxidative Stress Markers, and Clinical Profile in Relapsing–Remitting Multiple Sclerosis, *Antioxidants.*, 2023, **12**(8), 1638.
38 H. J. Weigmann, S. Schanzer, A. Patzelt, V. Bahaban, F. Durat and W. Sterry, *et al.*, Comparison of human and porcine skin for characterization of sunscreens, *J. Biomed. Opt.*, 2009, **14**(2), 024027.
39 J. Krutmann, A. Bouloc, G. Sore, B. A. Bernard and T. Passeron, The skin aging exposome, *J. Dermatol. Sci.*, 2017, **85**(3), 152–161.
40 H. Ibaraki, T. Kanazawa, C. Oogi, Y. Takashima and Y. Seta, Effects of surface charge and flexibility of liposomes on dermal drug delivery, *J. Drug Delivery Sci. Technol.*, 2019, **50**, 155–162.
41 M. B. R. Pierre and I. dos Santos Miranda Costa, Liposomal systems as drug delivery vehicles for dermal and transdermal applications, *Arch. Dermatol. Res.*, 2011, **303**(9), 607–621.
42 A. Mota, C. V. de, Z. M. F. Freitas, E. R. de, Júnior, G. M. Dellamora-Ortiz, R. Santos-Oliveira and R. A. Ozzetti, *et al.*, *In vivo* and *in vitro* evaluation of octyl methoxycinnamate liposomes, *Int. J. Nanomed.*, 2013, **8**, 4689.
43 N. R. Castro, C. Pinto, S. C. dos, V. E. B. de Campos, V. Cardoso, A. B. Vermelho and E. P. dos Santos, *et al.*, Development of hybrid vesicular nanosystems composed of lipids and chitosan for octyl methoxycinnamate encapsulation, *Colloids Surf., A*, 2021, **608**, 125476.
44 C. G. Morgan, S. S. Sandhu, Y. P. Yianni and N. J. F. Dodd, The phase behaviour of dispersions of Bis-Azo PC: photoregulation of bilayer dynamics via lipid photochromism, *Biochim. Biophys. Acta, Biomembr.*, 1987, **903**(3), 495–503.
45 T. L. Nguyen and M. A. Saleh, Thermal degradation of azobenzene dyes, *Results Chem.*, 2020, **2**, 100085.
46 E. Merino and M. Ribagorda, Control over molecular motion using the *cis–trans* photoisomerization of the azo group, *Beilstein J. Org. Chem.*, 2012, **8**, 1071–1090.
47 A. H. Heindl, J. Becker and H. A. Wegner, Selective switching of multiple azobenzenes, *Chem. Sci.*, 2019, **10**(31), 7418–7425.
48 A. Fagan, M. Bartkowski and S. Giordani, Spiropyran-Based Drug Delivery Systems, *Front. Chem.*, 2021, **9**, 720087.
49 Z. Zhang, Z. Xie, C. Nie and S. Wu, Photo-controlled properties and functions of azobenzene-terminated polymers, *Polymer*, 2022, **256**, 125166.
50 Y. Q. Yu, X. Yang, X. F. Wu and Y. B. Fan, Enhancing Permeation of Drug Molecules Across the Skin via Delivery in Nanocarriers: Novel Strategies for Effective Transdermal Applications, *Front. Bioeng. Biotechnol.*, 2021, **9**, 646554.
51 E. Larnac, A. Montoni, V. Haydont, L. Marrot and P. J. Rochette, Lipid Peroxidation as the Mechanism Underlying Polycyclic Aromatic Hydrocarbons and Sunlight Synergistic Toxicity in Dermal Fibroblasts, *Int. J. Mol. Sci.*, 2024, **25**(3), 1905.
52 N. Venkatarayappa, A. Athhar and M. Devi, Influence of Dissolved oxygen concentration on the production of superoxide dismutase in wild type saccharomyces mellis, *Asian J. Microbiol., Biotechnol. Environ. Sci.*, 2018, **20**(3), 928–934.